Marta Vidal Pereira

Bachelor in Micro and Nanotechnologies Engineering

Fabrication of 3D electrodes for biosensor applications

Dissertation submitted in partial fulfillment of the requirements for the degree of Masters in Micro and Nanotechnologies Engineering

Advisor: Prof. Drª Elvira Fortunato, Full Professor, Faculdade de Ciências e Tecnologias, Universidade Nova de Lisboa

Co-advisor: Prof. Drª Maria Goreti F. Sales, Adjunt Professor, Instituto Superior de Engenharia do Porto

FACULDADE DE CIÊNCIAS E TECNOLOGIA
UNIVERSIDADE NOVA DE LISBOA

Setembro, 2018

Fabrication of 3D electrodes for biosensor applications

"What you think, you become.
What you feel, you attract.
What you imagine, you create."

\- Buddah

Acknowledgements

É com um grande sentimento de satisfação e realização que entrego este trabalho. Estes últimos meses, embora complicados, foram os mais importantes do meu percurso académico. E como um percurso destes não se consegue fazer sozinho, não quero deixar de agradecer a todos os que direta ou indiretamente me acompanharam.

Em primeiro lugar, quero agradecer à minha orientadora, professora Elvira Fortunato, por todas as oportunidades que me proporcionou durante o curso e durante a tese, por ter aberto esta ligação entre o CENIMAT e o Biomark e por se ter sempre revelado disponível e interessada no meu trabalho. Também agradeço à minha co-orientadora, a professora Goreti Sales, por me ter aceite no seu centro de investigação, ter feito com que a participação no projeto europeu IBEROS fosse possível e a cima de tudo, por ter acreditado no meu trabalho e ter sempre uma palavra amiga a dizer.

Também agradeço ao professor Rodrigo Martins, por em conjunto com a professora Elvira Fortunato terem fundado este curso e abrirem as portas para sermos os "Engenheiros do Futuro".

À Carolina Marques, quero agradecer-te por me teres aturado nestes últimos meses e por teres sido minha amiga, mesmo quando eu não acreditava que era possível escrever esta tese. Obrigada por me teres acompanhado e teres sempre uma solução para me dar.

À Felismina Moreira, por ter sido a minha responsável no Biomark, por me ter dado todo o apoio possível e por ter tido paciência comigo, mesmo quando eu não percebia nada de AutoLab e eletroquímica. Muito obrigada por tudo o que me ensinaste.

A toda a equipa do CENIMAT e do Biomark, por terem estado sempre disponíveis para mim, à Sónia Pereira e Alexandra Gonçalves por aturarem os meus pedidos de última hora, à Ana Rita Cardoso e Daniela Oliveira por se terem tornado minhas amigas e me fazerem sentir em casa, mesmo a 350 km de casa.

Aos meus amigos da faculdade, obrigada por tornarem toda esta experiência mais suportável e por me terem feito gostar de cerveja. Aos meus coleguinhas de grupo favoritos, André Moura e Miguel Pinheiro, adoro-vos para sempre e obrigada por tudo. À minha família de praxe linda e disfuncional. Aos meus afilhados perfeitos: Maria Duarte, Bernardo Caetano, Francisca Tavares e Mariana Rodrigues e a todos os outros que estiveram sempre lá: Manuel Matos, Dmytro, Gui, Inês Tavares, Glória, Carolina, Catarina, Nuno. Foram das melhores coisas que a faculdade me deu e vocês sabem disso! Um obrigada especial às minhas amiguinhas, Maria Duarte e Francisca Tavares por todas as experiencias e momentos e à Mariana Rodrigues e Mariana Cortinhal por todo o "Mandatory Hate".

Sem esquecer claro dos meus amigos de Lisboa, que estão cá desde sempre, obrigada por todos os cafés, por me manterem sempre a ser eu e por não me terem esquecido mesmo quando não fui para o Técnico e vim para "Marrocos", Joana, André, Rafa, Pedro, Iko, Russo, Reis, Duarte e Sérgio adoro-vos.

Aos meus gordos do cinema, Leonor, Bia, Chico e Bruno, obrigada por serem os melhores amigos que podia ter encontrado a 50km de casa. Há coisas que não se conseguem explicar e vocês são uma delas, por todas as viagens inesperadas e kilos de pipocas, um obrigada enorme.

Nada disto seria possível sem as pessoas a quem devo literalmente tudo, os meus pais. Obrigada pela confiança enorme que têm em mim, por me terem ajudado e por serem os melhores "role-models" de sempre. Um obrigada enorme à minha irmã, por às vezes ser a irmã mais velha e por me fazer sentir a melhor pessoa do mundo. Quero também agradecer e dedicar a minha tese aos meus avós, aos quatro, por mesmo não conseguindo acertar com o nome do meu curso, terem um orgulho enorme em mim e nunca me deixarem ir abaixo.

Por fim, quero agradecer ao melhor que a faculdade me deu, Tomás Fernandes, não há palavras para dizer o quanto te agradeço por teres estado sempre presente. Obrigada pela amizade e por acreditares em mim, sem ti tudo seria mais difícil.

Resumo

A doença de Alzheimer é uma das formas mais comuns de demência, que afeta milhões de pessoas em todo o mundo. Esta doença embora incurável, carece de uma forma fácil e eficaz de diagnóstico.

Esta dissertação tem, por isso, como objetivo desenvolver um biossensor eletroquímico para a deteção precoce da doença de Alzheimer, através do reconhecimento de um biomarcador associado a diferenças visíveis no tecido cerebral e responsável pela criação de placas, o peptídeo Aβ-42.

Os sensores criados foram construídos com uma abordagem *bottom-up*, usando papel como substrato, uma vez que este material é um dos mais promissores na indústria da eletrónica flexível, por ser ecológico, barato, abundante, oferecer processos de construção biocompatíveis, fáceis e rápidos.

Os biossensores baseiam-se em elétrodos de carbono impressos, aliados a técnicas de laser. O circuito elétrico é composto por uma tinta condutora de carbono ou lápis 9B, impressa ou pintada num substrato de papel. O reconhecimento é feito por um polímero de impressão molecular que foi criado na superfície do elétrodo por eletropolimerização. Para este efeito, usou-se uma mistura de biomarcador alvo (Aβ-42) e monómero (*O*-Fenilenodiamina) e aplicou-se uma gama de potencial adequada para formação de um polímero condutor com zonas de reconhecimento por afinidade para o biomarcador escolhido. Vários parâmetros de eletropolimerização foram otimizados antes da construção dos dispositivos finais através da impressão do péptido, crescendo o polímero em volta do péptido Aβ-42 e removendo-o mais tarde, usando incubações com uma enzima e ácido adequados.

O desempenho do biossensor foi avaliado por técnicas eletroanalíticas. A resposta do biossensor foi estudada entre 0,1 ng/mL e 1 µg/mL de Aβ-42, em PBS buffer e Cormay serum. A reposta obtida indicou uma resposta analítica controlada dentro dos parâmetros fisiológicos desejados, considerando que um indivíduo saudável apresenta valores próximos a 23,3 pg/mL.

O biossensor apresentado oferece inúmeros benefícios, como o seu baixo custo de produção, a possibilidade de reutilização, eleva reprodutibilidade e resposta rápida, características que podem ter um forte impacto na deteção da doença de Alzheimer.

Palavras-chave: Biossensor; Eletroquímica, Papel; Alzheimer

Abstract

Alzheimer's Disease is one of the most common forms of dementia, affecting millions of people worldwide. Although incurable, an easy and effective form of diagnosis is still missing.

Thus, this work aims to develop an electrochemical biosensor for the early detection of Alzheimer's disease, by recognizing the peptide Aβ-42, a biomarker associated with visible differences in the brain tissue and responsible for the formation of senile plaques.

The intended sensing devices use a bottom-up designing approach, having paper as substrate. Paper is one of the most promising materials in the current flexible electronics industry, for being eco-friendly, cheap, abundant and offering biocompatible, easy and fast construction procedures.

The biosensors produced herein use pencil and printed carbon electrodes, allied with laser writing techniques. The electrical circuits are designed either on a conductive carbon ink or a 9B pencil tracks, printed or draw directly on the substrate.

The recognition is done by a molecularly imprinted polymer, created on the electrode's surface by electropolymerizing a mixture of the analyte (Aβ-42) and a monomer (*O*-Phenylenediamine). This process forms a conductive polymer with recognition sites displaying affinity for the selected biomarker. The parameters involved in the electropolymerization were optimized, by imprinting the peptide on the sensing layer, growing the polymer around the Aβ-42 peptide and removing it later by incubating in suitable enzyme and acid solutions. The performance of the biosensor was evaluated by electroanalytical techniques.

The analytical features of the biosensor were further evaluated by electroanalytical techniques. For this purpose, the analytical response was tested with standard solutions ranging from 0.1 ng/mL to 1μg/mL of Aβ-42 in PBS buffer and Cormay Serum. The response was found of analytical interest, considering that healthy individuals show normal values of ~23.3 pg/mL.

Overall, the developed biosensor offered numerous benefits, such as being a low cost, having reusability features, with a reproducible and fast response, which may have a strong impact in the early detection of Alzheimer disease.

Keywords: Biosensor; Electrochemical, Paper; Alzheimer

CONTENTS

List of figures

List of tables

Acronyms

a.u.	Arbitrary units
AD	Alzheimer Disease
AFM	Atomic Force Microscopy
APP	Amyloid precursor protein
ATP	4-Aminothiophenol
Aβ	Amyloid β peptide
CA	Chronoamperometry
CE	Counter electrode
CENIMAT	Centre for Materials Research
CI-HME	Carbon Ink Homemade Electrodes
CSF	Cerebrospinal fluid
CV	Cyclic Voltammetry
EDOT	3,4-Ethylenedioxythiophene
EIS	Electrochemical Impedance Spectroscopy
FWHM	Full width at half maximum
LDW	Laser Direct Writing
MIP	Molecularly Imprinted Polymer
NIP	Non-molecularly Imprinted Polymer
OP	Office Paper
oPDA	o-phenylenediamine
PBS	Phosphate buffer saline
PEDOT	poly(EDOT)
P-HME	Pencil Homemade Electrodes
POC	Point of care
PPI	Pulses Per Inches
RE	Reference electrode
RGB	Red, Green and Blue
SEM	Scanning Electron Microscopy
SWV	Square Wave Voltammetry
WE	Working electrode

XPS   X-ray photoelectron spectroscopy

XRD   X-Ray Diffraction

Symbols

μm	micrometre
Al_2O_3	Aluminum Oxide
$CaCO_3$	Calcium Carbonate
Fe^{2+}	Ferrous ion
Fe_2O_3	Iron (III) Oxide
Fe^{3+}	Ferric ion
$K_3[Fe(CN)_6]$	Potassium hexacyanoferrate III
$K_4[Fe(CN)_6]$	Potassium hexacyanoferrate II trihydrate
KCl	Potassium Chloride
M	Molar
mL	millilitre
mm	millimetre
mV	millivolt
NaCl	Sodium Chloride
Rct	Charge Transfer Resistance
Rs	Sheet Resistance
SiO_2	Silicon Dioxide
V	volt
Ω/□	ohms/square

Motivation and objectives

The aim of this master thesis is to develop a new form of early diagnosis and monitoring, in a simple, low-cost and reliable way, of Alzheimer Disease.

A crucial factor for the prevention and treatment of diseases is their correct diagnosis, and with Alzheimer's an easy and affordable method of diagnosis is still non-existent. Alzheimer's disease affects over 45 million people worldwide and this number is estimated to double every 20 years in aging populations, thus reaching a value of 115.4 million in 2050. Early detection of this disease, as well as the capability to distinguish it from other forms of dementia, is key to plan timely caring actions and help families intervene before the disease becomes too serious.

This project presents a new form of early diagnosis and monitoring, using a simple paper-based biosensor. This biosensor has carbon-based electrodes combined with plastic antibodies, which use the principles underlying the immune system, to detect the presence of biomarkers associated with the disease, without requiring invasive procedures. It seeks to measure the levels of $A\beta$-42, a peptide associated with the formation of plaques in the brain tissue, and that will work as the biomarker in this project.

Thus, the main goal is to create a device that can be cheap and eco-friendly, but still effective. For this purpose, two types of carbon-based materials are tested: pencil and a commercial carbon-ink. Although both materials are conductive, this project also focused on improving their conductive proprieties by laser technology.

In terms of structure, the thesis is divided in two main parts:

(a) the production/optimization of paper-based sensors with pencil and carbon ink electrodes;

(b) the functionalization of these sensors, with plastic antibodies capable to detect selectively $A\beta$-42.

1) Introduction

1.1)   Alzheimer Disease

Dementia involves a decline in cognitive skills used to perform every-day activities. The Alzheimer Disease (AD) is the most common form of dementia, with 60-80% cases of dementia being attributed to AD and affecting over 45 million people worldwide [1], [2]. Although symptoms can vary widely, the first problem many patients notice is forgetfulness, severe enough to affect their ability to function at home or work. However, the changes take place in the brain long before the signs of memory loss.

AD pathogenesis is complex, involving abnormal amyloid-β (Aβ) metabolism, Tau hyperphosphorylation, oxidative stress, reactive glial and microglial changes, and other pathological events [3]. In a patient with this disease, the brain has visible differences in its tissue, in the form of misfolded proteins called plaques and neurofibrillary tangles that are responsible for breaking down the brain's structure. Plaques are deposits of protein fragment (Aβ) that build up in the spaces between nerve cells, while tangles are twisted fibers of Tau proteins that build up inside cells [3]. Though autopsy studies show that most people develop some plaques and tangles as they age, those with AD tend to develop far more and in a predictable pattern, beginning in the important areas of memory, before spreading into other regions.

The diagnosis of AD is done typically via extensive clinical examinations based on specific clinical diagnostic criteria. This process involves several exams that aren't always reliable [4]. The identification of relevant biomolecules that could act as AD biomarkers, and therefore allow rapid and effective diagnosis of this disease, is highly pertinent. The amyloid precursor protein (APP), which is composed by amyloid β peptide (Aβ), is therefore the chosen biomarker for this project's device. The commencement of neurodegenerative disorders is known to be directly linked to high levels of Aβ-42/ Aβ-40 ratio, where Aβ-42 is the long form of the Aβ peptide and Aβ-40 is the shorter chain [5].

Although there is no cure, an early diagnosis is still one of the most important tools to fight the progression of this disease. There are already forms of detection of this biomarker such as ELISA [6], [7] and biosensors utilizing surface plasma resonance [8], [9], field effect transistor [10] and others[11] that have been reported to demonstrate the detection of Aβ. Most of these forms of detection only take in consideration the detection in cerebrospinal fluid (CSF), which makes them invasive and some don't allow a point-of-care (POC) analysis [12]. A biosensor that could detect this biomarker in blood samples could allow a reduction of cost, portability, and an overall easier way to diagnose the disease.

1.2)   Biosensors

Biosensors are analytical devices that incorporate a biological/biochemical sensing element and a transducer, to deliver a quantifiable response. The interaction between the analyte and the recognition element should be selective and capable of generating chemical/physical changes that are monitored by a transducer [13].

The type of components of a biosensor, as well as its construction, depends on its application, in addition to the sensitivity, sample characteristics, cost and lifetime. Generally, the most important element of the device is the recognition element, as it determines its selectivity. The range of analyte concentrations for which the device is sensitive is often associated with the transduction system, so the proper choice of these elements is critical [13], [14].

The analytical signal can be measured using optical (colorimetric, fluorescence, luminescence and interferometric, calorimetric) [15] and electrochemical methods (potentiometry, amperometry, conductimetry/capacitive and impedimetric) [11], [16]–[18], calorimetric differential mass (piezoelectric/acoustic waves) [18] or magnetic methods [19]. In the health field, the most commonly used biosensors are electrochemical, from which the most well-known are the glucose measuring devices [20], [21].

1.2.1) **Electrochemical Biosensor**

Electrochemical biosensors are the most common type of biosensors used today due to their portability, cost effectiveness, small size, and easy use. All these features makes these perfect for POC devices [22].

The principle behind an electrochemical biosensor is that the electrons flow between the electroactive species and the electrode surface, producing a chemical reaction and changing in the electrical properties of the solution. These changes can be sensed and used both for qualitative and quantitative analysis [23].

Typically, electrochemical biosensors consist of an analyte, receptors, measurable signals, transducer and a data analysis system. Each of these has a different role within the biosensor. The analyte is a biological/chemical element that works as the target; it can vary from virus, bacteria, peptides, and others. The receptors are biological or chemical elements that have identical properties to the analyte; these must be compatible with each other in order to bind and interfere with current flowing (that generate the signal). A transducer is the element used to transfer and convert the signal into the data analysis system. Overall, this biosensor works in the form of an electrochemical cell, where the presence of electrodes and electrolyte become necessary [13]. These electrodes can be made from different kinds of materials, which leads to variations in terms of sensitivity and in the length of the detection time of the sensor. Ideal electrodes are highly sensitive and show a fast response time; examples of the best materials are gold, silver and carbon.

When building an electrochemical biosensor, the most common combination for the electrodes is a 3-electrodes system, with a reference electrode (RE), a counter electrode (CE) and a working electrode (WE). The RE is used to maintain a known and stable potential, so it must be kept at a distance from the reaction site. The WE acts as the transduction element in the (bio)chemical reaction, while the CE establishes a connection to the electrolytic solution so that a current can be applied to the WE. All of these should be both conductive and chemically stable.

Voltammetry is the analytical technique that monitors electrochemical biosensors, consisting of a potential sweep application and subsequent reading of the electrical current so generated. Depending on the waveform applied on the 3-electrodes system, various electro-analytical methods can be employed, such as Cyclic Voltammetry (CV), Chronoamperometry (CA), Square Wave Voltammetry (SWV) and Electrochemical Impedance Spectroscopy (EIS) [19].

In CV the potential is applied as a sweep/linear function of time. This method explores the behaviour of electroactive compounds and the mechanism of oxidation and reduction and it allows to verify the reversibility of systems, to determine the presence of chemical events associated to the transfer of charge and to verify the occurrence of adsorption of products in the electrode [19], [24].

SWV is a pulsed-voltammetry, in which the potential is applied by pulsing one potential to another, rather than sweeping. It allows the analysis through the shape of the current-potential curve, resulting from the application of a given potential that changes according to the pulse amplitude and duration. The obtained signal is the resulting current from both pulses. It exhibits excellent sensitivity and high rejection to capacitive currents. This measurement requires an initial time where the working electrode is polarized to a potential, where the redox reaction does not occur. The current-potential curves have a well-defined profile and are generally symmetric, since the currents are measured only at the end of each half-period and the variations in the height and width of the potential pulse are always constant, for a given range of potentials. The height of the peak produced is proportional to the concentration of the electroactive species [19].

Chronoamperometry is a time-dependent technique, used to study the kinetics of chemical reactions, diffusion processes and adsorption. In this technique, a potential step is applied to the electrode and the resulting current vs. time is observed [25]. Since the current is integrated over relatively longer time intervals, chronoamperometry gives a better signal to noise ratio in comparison to other amperometric techniques [19].

EIS is one of the best tools for monitoring changes occurring at the surface of the biosensor. In this technique, a small sinusoidal excitation signal is applied to the WE and the subsequent response is

measured. This assay allows quantifying the resistance or capacitance of the electrolyte at the WE surface. The Impedance is the proportionality factor between the phase potential and the phase current over time, measured in Ohm [19], [24].

1.3)   Molecularly Imprinted Polymer

In conventional assays, natural antibodies are used to interact in a selective way with a given target analyte. But these natural materials show several limitations, like high production costs and low chemical stability. In the presence of organic solvents or in other non-physiological conditions, such as high temperature, pH and high salt concentration, natural antibodies lose their functionality. An alternative approach is to substitute these materials of natural origin by synthetic materials that display similar properties (biomimetic materials) [26].

Plastic antibodies mimic the response of natural antibodies while being of synthetic origin. These are obtained mostly by molecularly-imprinted polymer (MIP) technology, where a polymer is grown around the target molecule as can be seen in Figure 1.1. The exclusion of the target from the polymerized matrix generates imprinted sites that match the size and shape of the target [26].
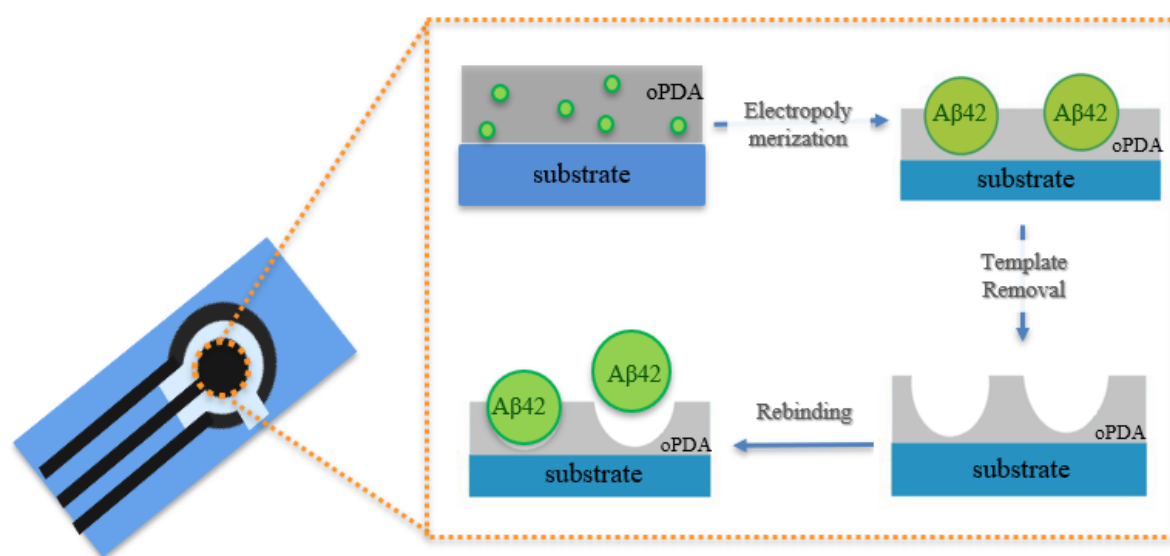
Figure 1.1 - MIP production steps. oPDA is the monomer used herein and AB42 the target biomarker.

These imprinted sites are expected to act similarly to natural antibodies, rebinding to the target with great affinity and selectivity [26], [27]. The use MIP and plastic antibodies allows the achievement of the artificial moulding of the analyte much faster than with a naturally occurring recognition and response [28] [29]. When creating MIPs for proteins or peptides, in order for the molecular imprinting to be successful, it is essential to use molecules with high affinity to the target.

Since the MIP will be part of an electrochemical sensor, the polymer may be produced by electropolymerization. This method allows to adjust several parameters that regulate the rate of polymer nucleation and growth and to control the film thickness and morphology [30]. The template particles and the monomers are mixed in the same solution and create the polymeric matrix directly on the sensor surface when the required electrical conditions are applied.

1.4)   Paper Electronics and Carbon Electrodes

Paper is the cheapest and most widely used flexible substrate in day-to-day life. It has a significantly lower price than plastic substrates and it also presents the advantage of being recyclable and made from reusable raw materials [31].

The idea of "printing" electronics on flexible substrates, such as paper or polymeric materials, is not new but only recently there have been promising reports of electronic devices fabricated directly onto

paper substrates [32], [33]. Paper has a porous structure and a large surface roughness. It can show fibres with different sizes and shapes, depending on their origin and treatments [34].

The lack of medical care in poor-resource countries and the constant need for renewable/reusable materials has opened doors for paper as a substrate for biosensing. Paper is easy to fabricate, mass-producible and disposable, so it makes sense to develop an easy-to-use, rapid and inexpensive POC device with this substrate [35], [36]. However, its hydrophilic nature makes it unsuitable for electrochemistry, at least in its natural form. In order to create a biosensor capable of sustaining electrochemical procedures, the substrate was hydrophobized using a wax coat as in microfluidic devices [35]. Wax printing is a method that requires only two steps, the printing patterns of wax on the paper surface and the melting of the wax into the paper to form a hydrophobic barrier. This technique is adapted to fabricate large numbers of paper devices in a single batch, due to its rapidity and low cost [37], [34].

There are thousands of conductive materials that can work as electrodes, but the most abundant is carbon. Carbon comes in numerous varieties of forms and has an extensive application in electrochemical studies [38],[39],[40]. When compared with metal electrodes, carbon has many advantages due to its low cost, wide range of potential windows and high chemical stability. This element exists in many allotropic forms such as graphite, graphene and diamond [41]. The most common form is based on the graphite structure, which can be modified or enhanced by surface treatments and modifications. These approaches can increase surface roughness, surface area or oxygenate functional groups on the electrode surface.

Graphite has both metallic and non-metallic properties, being very useful as an electrode material. The pencil graphite leads are composite materials containing graphite (~65%), clay (~30%), and a binder (wax, resins, or high polymer) [42]. According to the European Letter Scale, graphite pencils are marked with numbers, indicating the degree of hardness or blackness from 9H (the hardest) to 8B (the softest), and letters H (hardness) and B (blackness). The B-type leads contain more graphite and are softer, and the harder H-type leads have more clay, whereas HB type pencil leads contain equal portions of graphite and clay. Worldwide, 4% of graphite is used to produce pencils consisting of a fine powder in an inorganic (resin) or organic matrix (clay or a high polymer).

1.5)   Laser Direct Writing

Carbon based materials are very commonly used as electrodes for electrochemical assays for their intrinsic properties, attributed to the structural properties of carbon itself [43]. From all these, graphene and graphene derivatives have emerged as the most promising materials, due to their outstanding electrochemical properties, such as high conductivity, large surface area and mechanical robustness [44].

These materials can be produced by numerous deposition techniques, such as RF sputtering, screen-printing, inkjet printing, spin-coating, among others. All these methods offer numerous advantages, however they are rather expensive and have prolonged processes with several fabrication steps. Thus, during the past decades, alternative techniques have been studied and Laser Direct Writing (LDW) showed great potential [45].

LDW consists in an easy and simple method of obtaining patterns on the surface of diverse materials ranging from common precursors, like paper and cloth to polymers and metals, always under ambient conditions [45]. This procedure is done by a laser, a highly amplified and focused beam of radiation, which enables high accuracy and resolution printing, freedom of design, fast fabrication with very limited steps, complex micro and nanofabrication. It even excludes the necessity of lithography masks and clean-room equipment. All these characteristics make LDW a very cheap and fast alternative [46]. When carbon-based materials are printed by laser direct writing one more advantage is presented, since the laser beam can promote structural or chemical changes in the substrate, instead of ablation: the formation of graphene films. This has been demonstrated in several studies with multiple carbon precursors, like paper, Kevlar or Kapton [45]. The ease of obtaining high quality porous graphene films on the surface of substrates will surely allow many new electronic applications and electrochemical sensors [47], [48], [49].

2) Materials and Methods

This work is divided in two main parts. The first one consists in the production and optimization of carbon-based electrodes, using a CO_2 infrared laser cutting system as a tool for fabrication and improvement of conductive proprieties of the materials. In the second part, an electrochemical biosensor is produced by integrating a MIP material as biorecognition element.

This chapter begins with a brief description of the materials and equipment used, followed by a description of the experimental procedures involved in this work.

2.1.1) Pencil electrodes

For the fabrication and study of this type of electrode support, two types of paper were used: Whatman no. 1 chromatography paper (GE Healthcare, 87 g/m², 570x460 mm sheets) and office paper (OP) (Navigator, 80 g/m^2, 210x297 mm sheets). The pencils tested were from DERWENT Graphic and ranged from 3H to 9B (hardest to softest).

Before using a regular sensor design, tests were made to the pencil and paper, using a simple matrix where the different types of pencil had one to four layers (C), as can be seen in Figure 2.1a. Using a Universal Laser System CO_2 VLS 3.5, a pulsed cutting laser (wavelength of 10.6 µm), associated with a plano-convex lens (focal length of 50.8 mm, spot size of 0.127 mm) a change in the graphite structure can be made. The laser interface allows the definition of all laser parameters such as the laser power, the speed and the number of pulses per inches (PPI) in the form of a Red, Green, and Blue (RGB) color code.
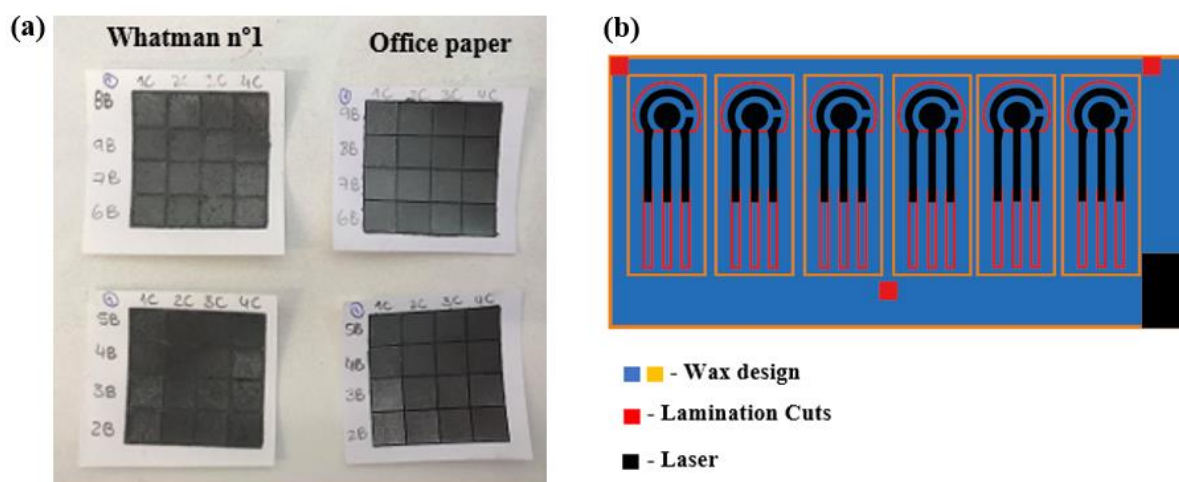
Figure 2.1- (a) Study of pencils and type of paper, effects of laser in different layers. (b) Adobe Illustrator Design

The results were monitored by four-point probe measurements and a multimeter.

When the laser parameters were optimized, and a conclusion could be made about which pencil and paper substrate were better, the next step consisted in applying these to a classical 3-electrodes design, for the construction of the electrochemical biosensor. Due to this application, the paper needed to show a hydrophobic behavior, for which a wax treatment was made on the substrate.

Adobe Illustrator was used to create the computerized design shown in Figure 2.1b. A Xerox ColorQube 8570 wax printer was used to apply the hydrophobic layer on the substrates. After printing, the wax needs to diffuse throughout the fibers of the paper; for this purpose, a hot plate annealing stage was done in a SCHOTT ROBAX equipment, for 2 minutes, at 120 ºC.

An acetate mold was created using the ULS and the Adobe Illustrator software, to produce identical electrodes. With the paper substrate glued to the mold, pencil electrodes were created by applying 4

layers of pencil 9B. After that, the mold was detached and the chips were displayed and organized in the laser table using the alignment marks as can be seen in Figure 2.1b; the best condition for this type of electrodes (also named as chips) was 4W Power, with a 0.2286m/s speed with the table at -0.2''.

To keep the chips protected and to create a distinguished area between the electrodes and the contacts, the chips were laminated according to Figure 2.1b. Silver ink from Conductive Compounds was used to coat the contacts in order to improve the readings of the chips. A hot plate annealing stage was then done for 20 min, at 120 ℃, to evaporate the solvents. The samples considered for this study were Pencil Homemade Electrodes (P-HME).

2.1.2) Carbon Ink electrodes

For the fabrication of these electrodes, carbon ink from Conductive Compounds was used. The paper substrate had the same treatment as the previous chips, but instead of using moulds, the substrate was laminated and then coated with two layers of commercial carbon ink, followed by hot plate annealing, for 20 min, at 120ºC. The samples considered for this study were Carbon Ink Homemade Electrodes (CI-HME).

2.1.3) Characterization of the home-made electrodes

Both electrodes were characterized by SEM-FIB using a Carl Zeiss AURIGA CrossBeam workstation instrument SEM images were captured in in-lens mode, with an acceleration voltage of 2 kV and an aperture size of 30 µm. Samples were glued onto aluminum substrates using a double-sided carbon tape and were coated with a thin carbon layer (<20 nm) using a Q300T D Quorum sputter coater.

EDS analysis was performed in a Hitachi TM 3030Plus Tabletop SEM, in low vacuum conditions for the identification of clay and graphite proportions in the composition of the different used pencil leads, as well as any other existent components.

The external layers of the electrodes surface were chemically and electronically analysed by X-ray photoelectron spectroscopy (XPS) to unfold the effects of laser ablation. The used equipment was an AXIS Supra XPS from Kratos Analytical and the used parameters were monochromated Al Kα radiation and pass energies ranging from 5 to 40 eV. The deconvolutions were done with CasaXPS. The asymmetric line shape was A(0.4,0.38,20)GL(30), whereas the symmetric ones were all GL(30). The full widths at half maximum (sp^2: 0.5, π to π^*: 2.7, sp^3 and carbon-oxygen bonds: 1.2-1.3) and the relative peak positions were held constant for all samples.

The crystallinity and structure of the samples were obtained by X-Ray Diffraction (XRD), PANalytical, model X'Pert Pro, in Bragg-Brentano geometry with Cu Kα line radiation (λ=1.5406 Å). The diffractograms were acquired in a range of 2θ ranging from 10 to 70 ° with a range of 0.03 °.

Raman spectroscopy data was generated by a Renishaw Qontor Raman microscope, equipped with 532 and 633 nm lasers, spectral resolution of 0.3 cm^{-1} (FWHM), mapping capability with 100 nm of lateral resolution and real time dynamic AUTO FOCUS.

Atomic force microscopy (AFM) measurements were performed in an Asylum Research MFP-3D Standalone operated in alternate contact mode in air (commonly known as tapping mode), using commercially available silicon AFM probes (Olympus AC160TS; k = 26 N/m, f0=300 kHz). The resulting topographies were plane fitted in Igor Pro software (Wavemetrics) and the final images generated using Gwyddion software.

2.2) Electrochemical sensor

2.2.1) Apparatus

The electrochemical measurements were conducted with a potentiostat/galvanostat from Metrohm Autolab, PGSTAT302N, equipped with a FRA2 module and controlled by Nova 10.1 software.

The interface between the electrodes and the Autolab was made through a homemade interface devic, specially designed by CENIMAT for this purpose. The fabrication protocol and pictures of the interface are shown in Annex A (Figure A.0.1).

2.2.2) Materials and Reagents

The materials and reagents used are listed in Table 2.1. All chemicals were of analytical grade and de-ionized water (conductivity <0.1 µS/cm) was employed.

Table 2.1– Materials and Reagents used and their origin

Materials/Reagents	Origin
O-Phenylenediamine (oPDA)	Sigma-Aldrich
Trypsin solution 10x	Sigma-Aldrich
Potassium hexacyanoferrate III ($K_3[Fe(CN)_6]$)	Riedel-De Haën
Potassium hexacyanoferrate II ($K_4[Fe(CN)_6]$) trihydrate	Riedel-De Haën
Potassium chloride (KCl)	Merck
β-Amyloid (1-42), human, ≥ 95%	GenScript
Serum Cormay human	PZ CORMAY S.A.
Phosphate buffer saline (PBS)	Amresco
Absolute Ethanol (99.5%)	Pancreac
3,4-Ethylenedioxythiophene,97% (EDOT)	Alfa Aesar
4-Aminothiophenol, 96% (ATP)	Acros Organics
Oxalic acid dihydrate	Merck

2.2.3) Solutions

The electrical features of the sensing surface were followed by checking the electrical features of a standard redox probe composed of 5.0×10^{-3} mol/L $K_3[Fe(CN)_6]$ and $K_4[Fe(CN)_6]$, prepared in PBS 1.0×10^{-2} mol/L, pH 7.36.

A KCl solution of 0.1 mol/L was prepared in deionized water. This solution was used as solvent of an EDOT solution of 0.01 mol/L. A 5.0×10^{-3} mol/L solution of aminothiophenol was prepared with a 30% ethanol aqueous solution acting as solvent. The oPDA standard solutions of 5.0×10^{-5} mol/L were prepared in PBS buffer, pH 7.36.

To prepare a control sensing layer (non-imprinted polymer, NIP), the polymer was formed in the absence of the target protein. For this purpose, an oPDA solution of 50 µmol/L was electropolymerized. The MIP sensing layer was prepared similarly, by added 10µL of a solution of Aβ-42 (10 µg/mL concentration, prepared in PBS buffer, pH 7.36) to 990µL of the previous solution.

Calibrating solutions required the preparation of stock solutions of Aβ-42 oligomer. This was prepared in a concentration of 0.5 mg/mL, in PBS buffer, pH 7.4. The Aβ-42 oligomer was prepared according to Marco Gobbi *et al* [50], where the monomeric peptide solutions were diluted to 100×10^{-6} mol/L in 50×10^{-3} mol/L phosphate buffer, 150×10^{-3} mol/L NaCl, pH 7.4, and incubated for 24 hours at 4ºC. Less concentrated standards were obtained by accurate dilution of the previous solution in PBS buffer or in Cormay Serum.

For template removal two solutions were used: (a) Trypsin diluted 100x in PBS buffer, pH 7.36 and (b) Oxalic acid 0.05 mol/L prepared in deionized water.

2.2.4) Analytical Procedures

All assays were conducted in triplicate to ensure reproducibility. The first procedure in each chip was related to the reading of a blank signal (only buffer). This was necessary to ensure an analytical correlation within assays of chips from the same batch. The implemented procedures depended on the assembly of the chip, described next. The pencil (P) or carbon ink (CI) homemade electrodes (HME) were assigned as P-HME or CI-HME, respectively.

2.2.4.1) Carbon Ink Chips

CV and SWV measurements were conducted in the standard iron redox probe. For CV assays, the potential was scanned from -0.7 to +0.7 V, at 50 mV/s. For SWV studies, potentials ranged from -0.4 to +0.3 V, at a frequency of 10Hz, with a step height of 250 mV.

EIS assays were performed with the same redox couple solution $[Fe(CN)^6]^{3-/4-}$ with open potential circuit (OCP), using a sinusoidal potential perturbation with an amplitude of 0.01 V and a number of frequencies equal to 50, logarithmically distributed over a frequency range of 0.1-100 kHz. The impedance data was fitted with commercial software Nova.

After the first readings, a pre-treatment was conducted by CA, applying +1V for 10 seconds in the EDOT solution. Another reading was made to ensure that the layer of PEDOT was well-formed on the WE. Then, the chip was incubated in ATP for 1h. After this incubation stage, the electropolymerization was made by CV with either MIP or NIP preparing solutions. The potentials were scanned from -0.45 to +0.8 V, at 100 mV/s, in 5 consecutive cycles. The template removal procedure was made (in both, MIP and NIP sensing layers), by incubating the chip in Trypsin solution for 90 min at 36ºC, followed by another incubation in oxalic acid for 2 hours at room temperature.

The calibration curve was performed by SWV and EIS measurements. Readings were made for MIP and for NIP materials, with each assay performed at least 3 times. Each calibration curve was achieved after a 20 minutes incubation period for each Aβ-42 standard solution, and for increasing concentrations. Each Aβ-42 incubation was followed by an iron redox probe reading, extracting the electrical features of the surface for each standard concentration. The Aβ-42 concentrations ranged from 0.1ng/mL to 1.0 µg/mL, prepare in buffer.

Calibration assays were also conducted by incubating Aβ-42 standard solutions prepared in serum and followed by SWV measurements. For this purpose, Aβ-42 was prepared in Cormay serum solution, diluted 100 times, and in the same concentration range as before.

The chemical/physical data of the synthetic materials was obtained by surface analysis using Raman spectroscopy, SEM and AFM. The samples considered for this study were: PEDOT/CI-HME, MIP/PEDOT/CI-HME, trypsin/ MIP/PEDOT/CI-HME and NIP/PEDOT/CI-HME.

2.2.4.2) Pencil Chips

With this type of electrodes, a study was conducted to understand the best type of pre-treatment to be applied. The best pre-treatment ended up being the same as described in 2.2.4.1). The pencil homemade electrodes (P-HME) weren't electrochemically stable so no further procedures were applied. The samples considered for this study were: P-HME, P-HME/KCl, P-HME/NaCl, PEDOT/P-HME.

2.2.5) Characterization of the Sensors

Raman spectroscopy data was generated by a Thermo Scientific DXR Raman spectroscope, equipped with a confocal microscope and a 532 nm laser. A 5mW laser power at sample was allowed for 25 µm slit aperture.

Scan-electron microscopy (SEM) studies were performed on an FE-CryoSEM/EDS, from JEOL JSM 6301F, Oxford INCA Energy 350, Gatan Alto 2500 microscope, operating at 15 kV and 9.9 mm working distance.

Atomic force microscopy (AFM) measurements were performed in an Asylum Research MFP-3D Standalone operated in alternate contact mode in air (commonly known as tapping mode), using commercially available silicon AFM probes (Olympus AC160TS; k = 26 N/m, f0=300 kHz). The resulting topographies were plane fitted in Igor Pro software (Wavemetrics) and the final images generated using Gwyddion software.

3) Results and discussion

In this chapter, all the work regarding the biosensor fabrication and functionalization is presented and discussed. First, section 3.1) presents the substrate characterization, comparing the two types of paper studied. Secondly, section 3.2) shows the optimization results of laser parameters used to increase conductivity of P-HME, as well as a comparison between the two types of carbon-based materials used to serve as electrodes in this work (P-HME and CI-HME). Finally, section 3.3 presents the electrochemical characterizations of both types of sensor, with respectively studies and analysis.

3.1)   Paper Characterization

Two types of paper were used in the construction of the sensor: OP and Whatman nº 1. These papers are used herein as a support for casting the CI or P-carbon materials, making it important to know the morphological and crystallographic features of these supports.

SEM analysis of OP is shown in Figure 3.1a, where the surface displays a matrix of randomly dispersed long cellulose fibers of about 5 to 15 μm width. In addition, these fibers also seem flattened, probably due to the compression step during the manufacturing process.
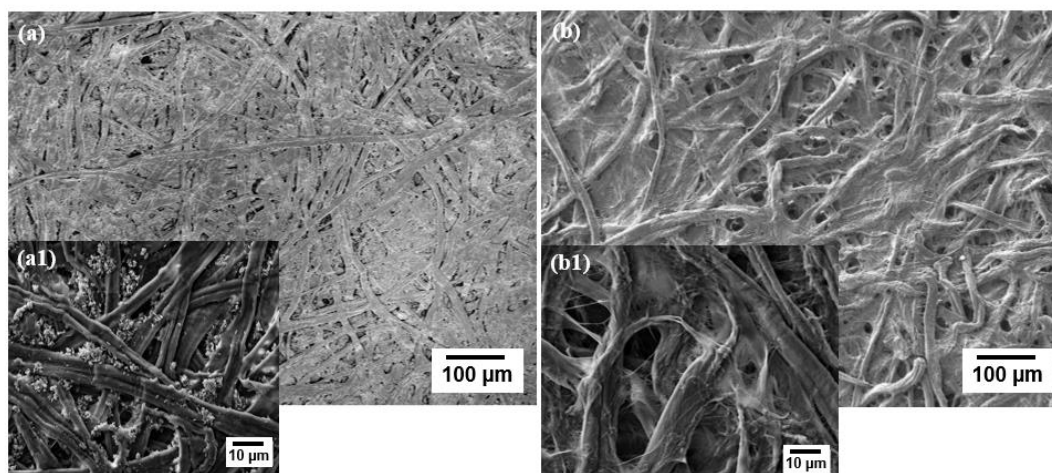
Figure 3.1- SEM images top view of (a) OP and (b) Whatman nº1.

In comparison, SEM images of Whatman paper (Figure 3.1b) demonstrate much larger fibers, ranging from 15 μm to 20 μm. Its surface, however, is less uniform due to the fact that Whatman paper is more porous and has lower fiber density than OP. Even though fibers are scarcer, they show a more cylindrical geometry that contributes to the bigger thickness of Whatman paper.

The structural analysis of the paper was made by X-Ray Diffraction, as can be seen in Figure 3.2.
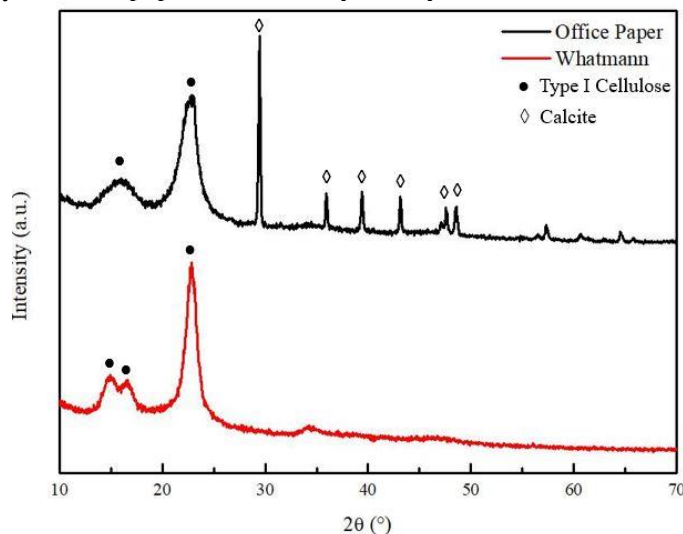
Figure 3.2 – Structural Characterization of Whatman n°1 (red) and OP (black) by XRD. Type I cellulose marked as ● and calcite marked as ◊.

By diffractogram analysis, it is possible to observe the characteristic peaks of type I cellulose (ICDD file: 00-056-1718719), marked as ●. In Whatman paper two peaks can be identified at 14.88° and 16.63°, which does not happen in the OP, where there is only a large peak 15.9°. This can be justified by the presence of more residual amorphous materials in its cellulose fibers, which create a fusion of the peaks. Type I cellulose has a monoclinic geometry, with unit cell constants a = 8.3, b = 10.3, c = 7.9 Å and angles α = 90, β = 84 and γ = 90 °.

When analyzing the OP diffractogram it is possible to identify another crystalline structure, marked as ◊ that is not present in Whatman paper. This structure is Calcite ($CaCO_3$) (IDD file: 01-072-1937); it has a rhombohedral geometry and unit cell constants a = b = 4,99 and c = 17,08 Å with angles α= 90, β = 90 e γ = 120 °. Calcite is the principal additive to this type of paper fabrication; it is also used to alter the optical properties of the paper forming porous agglomerates, is responsible for the opacity and gloss of this kind of paper and improves the ink reception capacity, so it is more used in substrates for writing and printing.

3.2) Carbon-based electrodes characterization

3.2.1) Pencil Characterization

Commercial pencil leads are made using graphite and clay and each one has a certain mixing ratio, which differs according to its hardness. While clay gives the hardness and works as a binder (H characteristics), graphite gives the B characteristics to a pencil which can be described as the blackness and softness. Higher hardness is directly related to an higher percentage of clay and lower percentage of carbon [44], [51], [52].

According to Y. Kim *et al* [51] clay's main contents are SiO_2, Al_2O_3 and Fe_2O_3, but it can vary according to the manufacturer. Since both percentage and actual composition are two unknown factors an EDS analysis was performed to the used pencils, ranging from 3H to 9B. Results can be seen in Figure 3.3.
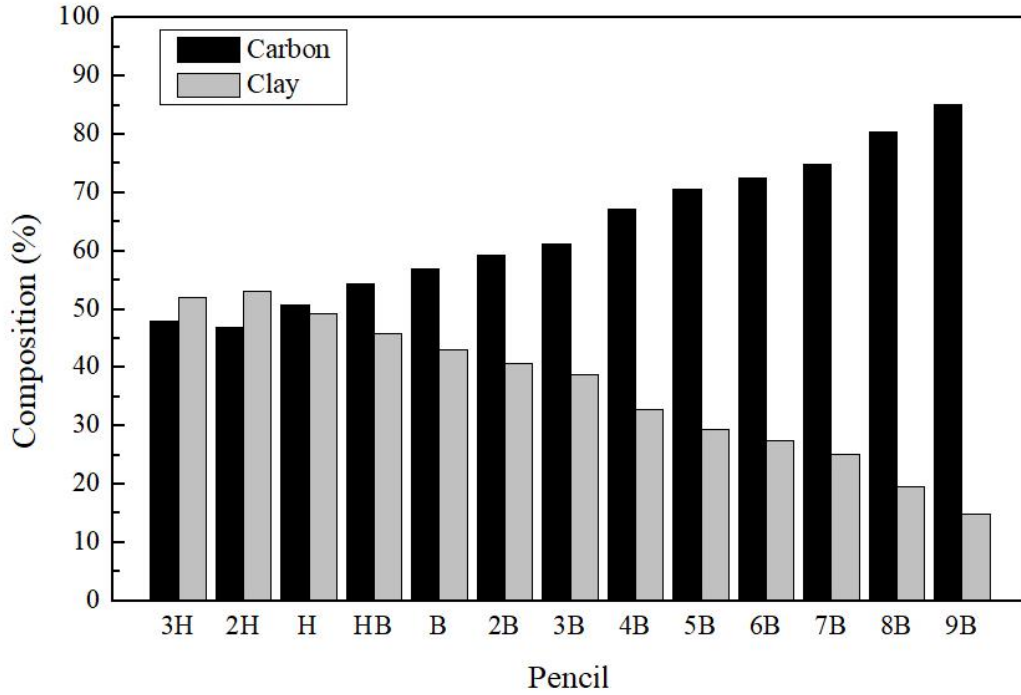
Figure 3.3 - Grade of lead pencil. H (for hardness) to B (for blackness). Results were normalized based on the carbon percentage. Clay composition comprises the percentages for aluminum, silicon, oxygen and residual calcium.

The obtained data was very similar to both Satoru Kaneko papers [33], [44], as the pencils became softer, they showed a visible increase in carbon proportion in its composition and 9B was highlighted has having the biggest carbon percentage of them all. On the other hand, pencils 2H and 3H showed the highest composition of clay and also had the highest percentage of aluminum.

The samples existing components were identified as carbon, silicon, aluminum, oxygen and had some residual calcium, all accordingly to R.N. Bhowmik paper [52]. The only missing element that was expected to be found through this EDS analysis was iron. Its absence can be justified by either the existence of such trivial amounts that the software did not consider it relevant or the manufacturer just does not apply iron(III) oxide in its clay.

The electrical conductivity of a pencil trace depends on the quality of the contact between graphite particles in the percolating network. Expansion and contraction of this network, induced by either mechanical stress or chemical interactions, should greatly affect the quality of inter-particle contacts and thus the overall electrical conductivity. Samples with the highest percentage of carbon are expected to work better as electrodes, since they should be more conductive.

3.2.2) Identification of laser parameters

The first studies were conducted with samples of different grades of pencil with different layers. Before any laser treatment, their sheet resistance (R_s) was measured with a four-point probe. In Annex B (Table B.0.1) are represented the values of R_s according to the type of pencil and layers used for pencils 9B to 2B since the others showed no resistance.

Sheet resistance was calculated using equation 1.

$$Rs = k\,\frac{V\,(mV)}{I\,(\mu A)} \tag{1}$$

Since the spacing between the probe points was constant and the sample was considered a thin film, the average resistance of the substance can be given by equation 1, with k being the constant for the average resistivity that is equal to 4.532, I the current and V the voltage.

Pencils 8B and 9B revealed the best sheet resistances (488.10 $\Omega/\square$ and 619.98 $\Omega/\square$, respectively) with no treatment as expected, since they had the lowest concentration of clay and higher concentration of graphite (carbon) [44], thus these were the chosen to proceed with the study. Since no studies about the effect of laser in pencil were found, a wide range of conditions was tested, which revealed better results for pencil 9B, as can be seen in Annex C (Figure C.0.2).

When analyzing the graph on Figure C.0.2, the strong influence of the substrate can be noticed. Four different regions were created:

- A region where the laser treatment did not make any impact on the sample's surface (grey area);
- A region where there was an improvement on R_s values (green area);
- A region where although there was an improvement on R_s the substrate was affected and created a sort of mesh (yellow area);
- And finally, a region where the sample was destroyed (red area).

OP showed a smaller area where laser treatment improved the samples R_s, so more conditions were tested. Even with a smaller area of improvement, better results were achieved with this type of substrate.

The samples were hand-made in a squared shape as mentioned in 2.1.1), so "human-error" had to be kept in mind.

With laser treatment, the best results achieved for each substrate are presented in Table 3.1.

Table 3.1 - Ideal Conditions for Pencil 9B samples in Office paper and Whatman n°1

Substrate	Laser Condition	Sheet Resistance ($\Omega/\square$)
Office Paper	Power: 3.5 W Speed: 0.138 m/s	29.911
Whatman n°1	Power: 2.5 W Speed: 0.127 m/s	37.162

OP is less expensive and easier to find than Whatman and, as the main goal was to produce a low-cost biosensor, it turned out to be the best choice as substrate. A hydrophobization step was required, considering that the hydrophilic nature of paper is not compatible with electrochemical biosensing applications, since any solution would be soaked by the substrate itself, provoking short-circuits between the electrodes.

The application of the wax layer to hydrophobize the paper, plus the change of pattern (Figure 3.4b) lead to variations in the laser conditions. Measurements of resistance started to be made with a multimeter due to the small area of the electrodes. To ensure similarity between measurements, resistance values were always taken in the WE with the multimeter probes separated by 0.3 cm. New conditions and respective resistances obtained can be seen in the color map on Figure 3.4a.
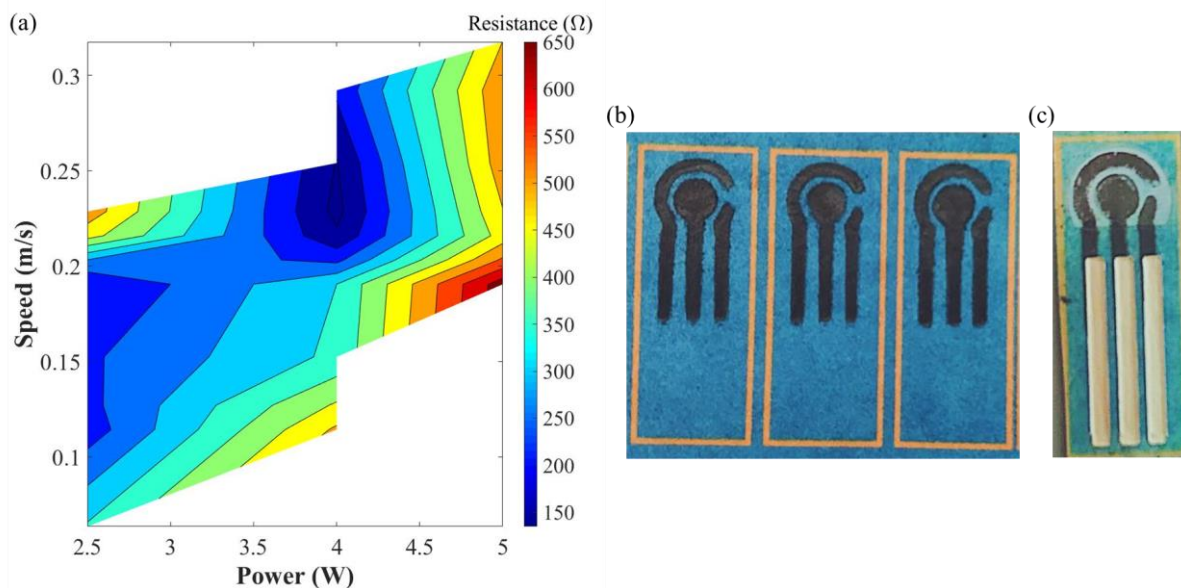
Figure 3.4 – (a) Resistance values with different speed and power conditions in hydrophobized OP with Pencil 9B samples. (b) Example of pencil 9B samples. (c) Final P-HME.

After analyzing the obtained results, it can be concluded that slower speeds and lower power lead mostly to better electrical properties. Although there is a significant area where resistance values are around 150 Ω, some lacked integrity and/or were inconsistent. The best condition consisted on 4 W of power and 0.229 m/s of speed, which presented a resistance of about 5% of its original value, making these the chosen parameters to produce the electrodes used in the stages ahead.

With the laser parameters established, the final step of production of P-HME was to encapsulate these using laminating sheets to prevent any damage and coat the contacts with silver ink to improve the electrical contact for the electrochemical readings (Figure 3.4c).

CI showed no need to have laser treatment, as it had 25.69 $\Omega/\square$ by itself and the laser only decreased its conductivity proprieties. An image of the final CI-HME can be consulted in Annex D (Figure D.0.3).

In order to understand and justify the effect of laser in pencil-based samples, morphological and crystallographic analysis were conducted, as can be seen in sections ahead.

3.2.3) SEM Characterization

Morphological characterization of pencil samples with and without laser irradiation and of CI-HME were made using SEM, as can be seen in Figure 3.5 and Figure 3.6 respectively.
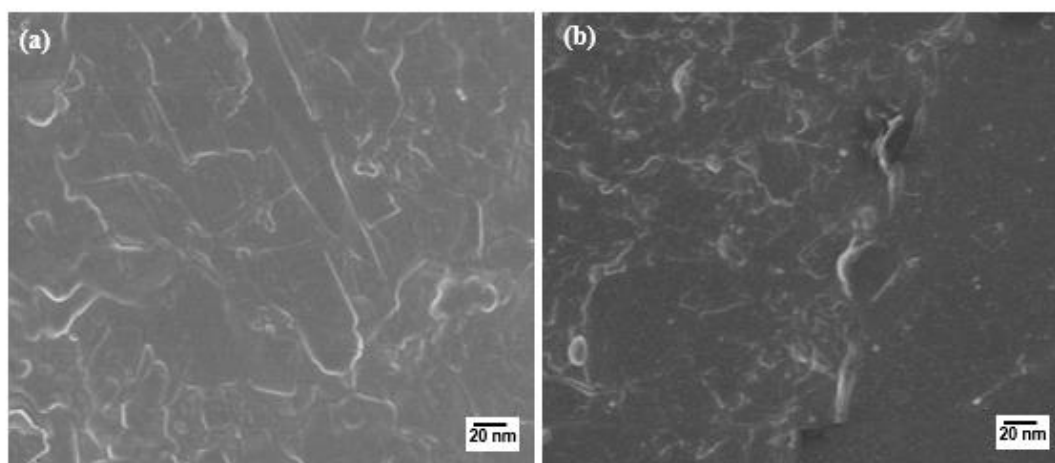
Figure 3.5 - SEM images top view: (a) Pencil in OP, (b) Pencil in OP after laser incidence.

17
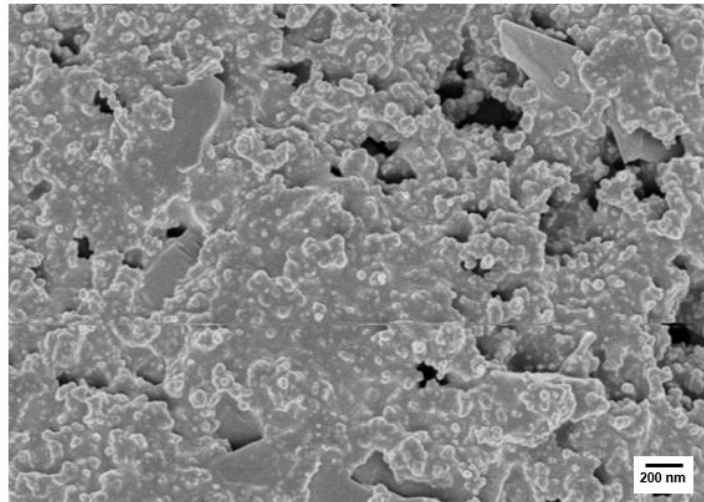
Figure 3.6 - SEM top view of CI-HME.

Since the chosen paper was OP and SEM images were taken in top view, Whatman samples were not taken in consideration. As can be seen in Figure 3.5, there are no visible significant surface changes with the laser incidence, at this magnification. Increased magnification images could show surface differences, but higher resolution could not be achieved due to technical limitations of the equipment at the time.

The CI-HME sample revealed a "grainy texture" despite resembling a continuous film. Some gaps and fissures can be observed, due to the production or annealing process. This morphology is similar to commercial chips, so it works as a good method of comparison.

3.2.4) EDS Characterization

In addition to the EDS analysis made in 3.1), another analysis was made to a 9B pencil sample with laser treatment, in order to understand if any modification occurred. Results can be seen in Figure 3.7 and Annex E (Figure E.0.4 and Figure E.0.5).
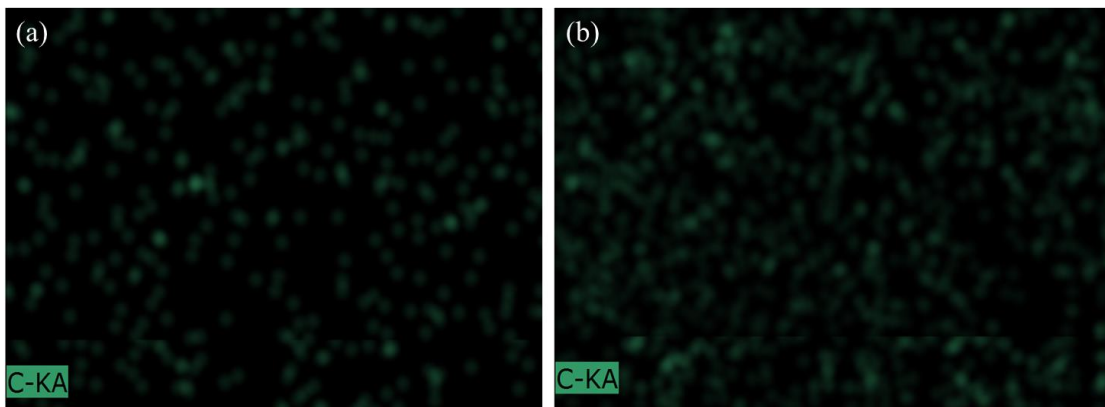
Figure 3.7 - EDS analysis of 9B pencil sample with and without laser treatment. EDS mapping of carbon in sample without (a) and with laser treatment (b).

EDS quantitative analysis showed that the area irradiated by the laser had a significant decrease in carbon content (from 85.11% to 79.89%), which could be due to the removal of some material from its surface. Although when comparing the mapping, the carbon appears to be more predominant in Figure 3.7b. This can be justified by the fact that the analysis is performed within a very small area of the sample, that may not be a good representative of its entirety or because the quantitative analysis is relative. Elemental percentages are calculated in function of the most abundant element, which can change from sample to sample.

The analysis found evident that the laser treatment leads to a change in atomic mass percentage of the components, since the same elements as the previous sample exist in less quantities: carbon, silica, oxygen, aluminium and residual calcium. The thermal effect of the laser treatment might have induced the formation of molten grains and micro cracks in the outer layers of the graphite surface, which would result in extreme physical stress and possible structural re-arrangement [53].

3.2.5) Raman Spectroscopy

To have a better understand of what the role of laser in the improvement of pencil's conductivity proprieties was, Raman Spectroscopy was used. The results can be seen in Figure 3.8.
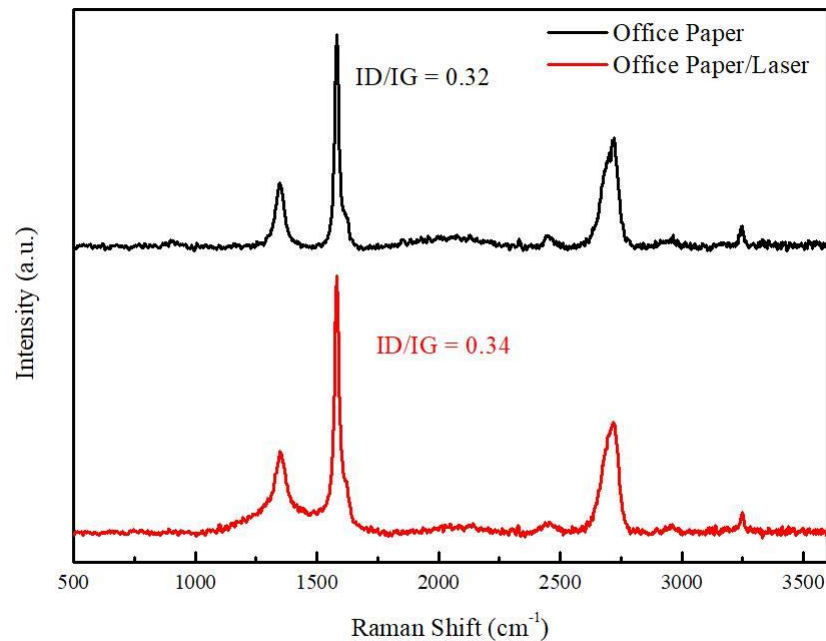
Figure 3.8 – Raman Spectra of OP with pencil 9B with and without laser treatment

The Raman spectra of all carbon systems showed only a few prominent features, no matter the final structure. These evidenced two intense bands (G and D) around 1500 cm^{-1}, corresponding respectively to natural graphite (1575 cm^{-1}) and the type of graphite material (1355 cm^{-1}), and few other second order modulations around 2700 cm^{-1}. The peaks shape, intensity and positions allowed distinguishing several forms of carbon from a metallic nanotube to amorphous carbon [54].

In general, the intensity ratio (I_D/I_G) is characteristic of the extent of disorder present within the material: the higher the ratio, the lower the disorder. The G band is the first-order Raman band of all sp^2 hybridized carbon materials. The D band is a defect activated band in sp^2 hybridized carbon materials. The intensity of the 1575 cm^{-1} line rises with the laser treatment, which is associated with an increase in the amount of sp^2 carbon [55], making a higher I_D/I_G ratio and justifying the increased conductivity of the sample.

3.2.6) XRD Characterization

X-ray diffraction was an essential tool to identify the crystalline phases of the graphite and compare with the other characterization methods, the results can be seen in Figure 3.9.

This technique helped to understand what the cause of the improvement of pencil conductivity was, whether a change of material occurred or only a crystallographic reorganization.
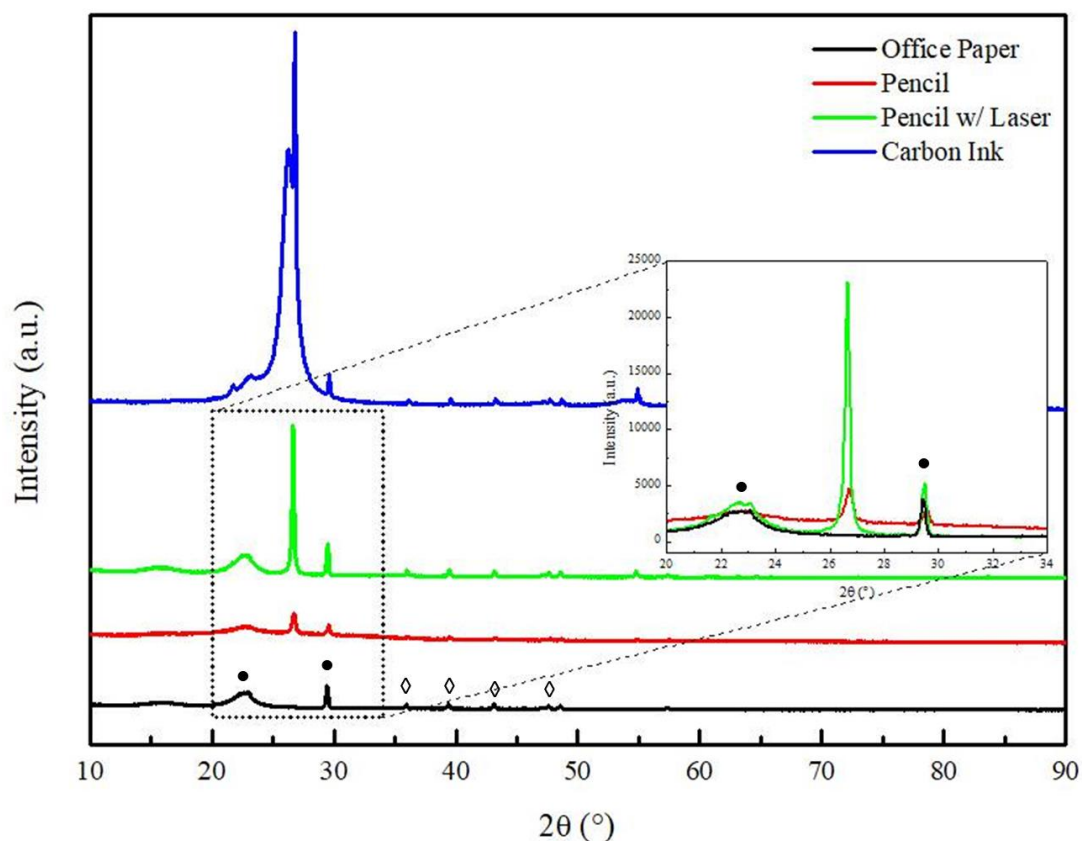
Figure 3.9 – XRD diffractogram of OP, 9B Pencil with and without Laser and Carbon Ink. Type I Cellulose marked as ● and Calcite marked as ◊

By analyzing the XRD diffractogram the presence of the spectrum corresponding to the paper substrate is clear, showing the characteristic cellulose and calcite peaks (marked as ● and ◊ respectively) as mentioned before in 3.1).

Apart from the presence of the substrate, another peak is visible at 26.6 ° corresponding to graphite (IDD file: 01-072-0961). This peak is present in both pencil samples but is more intense with laser treatment. The sample with no laser had a full width at half maximum (FWHM) of 0.3022 ° that decreased to 0.1877 ° with laser treatment. The increased intensity of the peak and decrease FWHM proved that there was a crystallographic organization of graphite, by induction of oxygen-containing groups by means of a physico-chemical reaction [52].

3.2.7) XPS Characterization

XPS can measure the elemental composition, empirical formula, chemical state and electronic state of the elements within a material. This technique helps to gather further information about the existing phases and oxidation states at the sample's surface that could not, otherwise, be obtained with XRD. Figure 3.10 presents the spectra obtained for 9B pencil samples with and without laser treatment. XPS elemental composition can be consulted in Annex F (Table F.0.2).
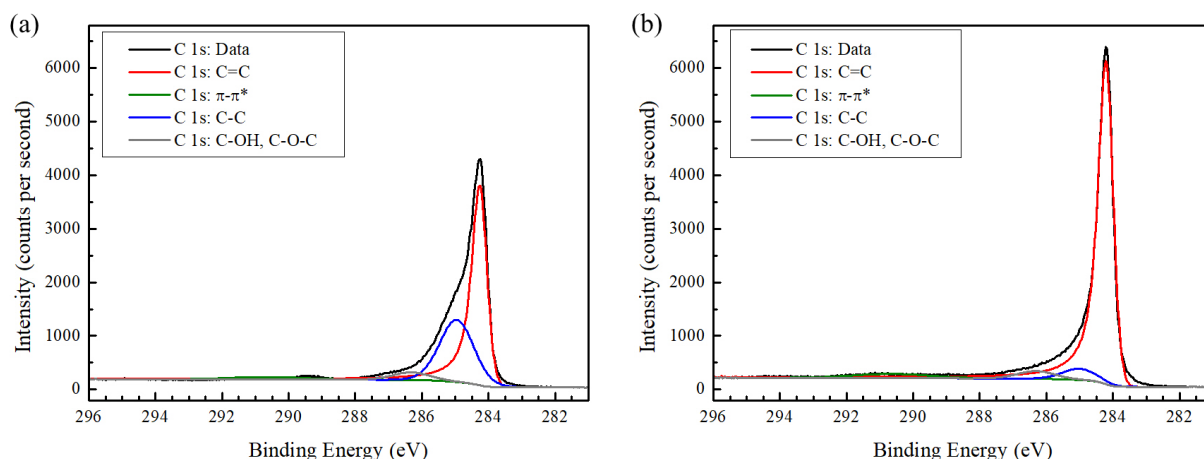
Figure 3.10 – C 1s region of XPS spectra of 9B pencil sample without (a) and with laser treatment (b).

The energies and intensities of the photoelectron peaks enable identification and quantification of surface elements, based on the unique binding energy each element has. The shift in binding energies of one element is due to different bonding situations (which is referred to as chemical shift).

The bond of carbon atoms can hybridize, to form σ and π bonds, in three different ways: sp^3 hybridization, which is a typical structure of diamond and silicon (C-C); sp^2 hybridization, which is a two-dimensional graphite layered structure (C=C) and sp^1 hybridization, that is a one-dimensional structure. Structure depends strongly on sp^2 and sp^3 bonds [56]. π bonds form only between sp^2 hybrids, are weaker than σ bonds and they are responsible for the electronic properties of the carbon films, namely their conductivity and optical bandgap. As for σ bonds, they define the mechanical properties of carbon films, such as their hardness, which is therefore linked with sp^3 hybrids [57]. So, an accurate measurement of the sp^2 and sp^3 hybrids concentration is desirable for understanding the properties of the carbon films.

Graphite and graphitic-like compounds have an asymmetric C 1s peak-shape (as they are conductive) centred at 284.5 eV. Also present, is the structure related to the π to $\pi*$ transition (shake-up) at around 286.4 eV [58], [59]. Deconvolutions of carbon C 1s peaks provide quantitative information regarding the binding modes of carbon. It is revealed that 9B pencil samples without laser treatment contain a significantly higher amount of sp^3 carbon (C-C) when compared to laser treated samples (15.99% compared to 2.99%). As the laser treatment lowers the amount of sp^3 carbon bonds, the sp^2 portion is increased from 76.61% to 90.16%.

The laser treated samples, due to their increased amount of sp^2 bonds, shown by the stronger intensity, have a higher electrical conductivity.

3.3)   Electrochemical Characterization

3.3.1) Pencil

The first approach was to verify the behaviour of the WE after its preparation. This was done by monitoring the electrical features of the oxidation/reduction peaks of the standard redox probe, by different electrochemical techniques. These readings identify the typical values of this iron probe, enabling a comparative study of the modifications made in the following steps to be carried out. These readings also helped to guarantee homogeneity within chips prepared throughout this work.

When the iron redox probe is followed by CV, the scan towards the positive potentials promotes the oxidation of iron, converting Fe^{2+} into Fe^{3+} and yielding a current flow from the solution species to the electrode surface. The reserve scan yields the opposite effect and the behaviour can be explained in an identical manner. For a purely reversible electrochemical reaction, which is the case of the current iron probe used herein, the recorded CV data show typically well-defined characteristics. From a current point of view, the ratio of the peak currents must be equal to one (meaning that the extent of the oxidation

reaction equals the extent of the reduction reaction), and the voltage separation between the current peaks must be 59 mV for a reversible process.

With this type of electrodes, the oxidation and reduction peaks of the iron probe were too far apart, indicating that the surface did not display enough conductivity properties for the intended application. To solve this, a pre-treatment or a cleaning step became necessary and were implemented. This is a common procedure used among electrochemical biosensing development, also used in commercial 3-electrodes devices.

3.3.1.1) Electrochemical study

The main purpose of the first study was to select a suitable pre-treatment or cleaning process that could improve the conductivity proprieties of the P-HME. In the literature, there are several papers using pencil-based electrodes, but never with laser treatment as this work was the first attempt to carry out such preparation of 3-electrodes systems. Yet, as the main target was to improve the carbon surface in terms of electrical output, the chosen parameters were based on Jayant I. Gowda *et al* [60] and Golnaz Parvizi-Fard *et al* [61] papers, relying mostly in electrochemical approaches in specific solutions. Herein, four solutions were tested: KCl 0.5 M and 0.1 M, NaCl 0.1 M and EDOT. NaCl studies can be consulted in Annex G (Figure G.0.6).

KCl Studies

To identify the best cleaning condition for this type of electrodes, the first study was made using a KCl solution 0.1M, as it had been used in several papers regarding graphite and other carbon-based electrodes [60], [62].

With a pre-treatment of the KCl solution by CV, several conditions were tested, the best conditions are shown in Figure 3.11a. With a potential range of [-2; +2] V, 40 cycles and 100 mV/s (CV1), CV analysis shows oxidation and reduction peaks of -0.35 V and 0.35 V, which indicated a *quasi-reversible* behaviour. Although the voltage separation indicated a quasi-reversible behaviour, the peaks were too separated and this pre-treatment was still not ideal for the purposes of this work.

Adding more cycles could make the electrode degrade and fewer cycles made little to no difference on the original reading. Changing the concentration of the KCl solution to 0.5 M (CV2) and keeping the same parameters made the peaks much closer, with a voltage separation of 105 mV.

Figure 3.11 - Pre-treatment of P-HME with KCl, (a) comparison between P-HME and two pre-treatments with CV; (b) comparison between P-HME and two pre-treatments with CA. Assessed in 5.0 mM $[Fe(CN)_6]^{3-}$ and 5.0 mM $[Fe(CN)_6]^{4-}$, in PBS buffer, pH 7.2.

In an attempt to reduce the time spent on CV assays and to try to obtain better results, a CA pre-treatment was studied and the results are shown in Figure 3.11b. With the 0.1 M KCl solution, the time

was fixed at 100 s and the extremes of the CV were studied 2 V (CA1), -2V (CA2). The obtained results did not lead to any improvements, so no further attempts were made.

With this solution, the best conditions found were CV2, but with EIS analysis the results showed irregular consecutive readings with an increased R_{CT} tendency (R_{CT} is the charged-transfer resistance, which corresponds to the diameter of the semi-circle observed in the Nyquits plots procedure by EIS readings). This can be justified by a constant removal of nanostructures from the WE external surface, promoted by the cleaning processes between reads.

EDOT Studies

The studies presented above were meant to clean the carbon surface but did not reach enough reproducibility. From the analysis of the EIS of several readings of the same chip, with the same treatment, the results tended to change, evidencing that the WE was changing. So, instead of cleaning, a thin layer of a conductive film was created on top of it, by using an EDOT solution. The poly(EDOT) is meant to improve the electrical properties, while stabilizing the particles at the surface by trapping them in the polymeric network. The two best results of each pre-treatment can be seen in Figure 3.12.
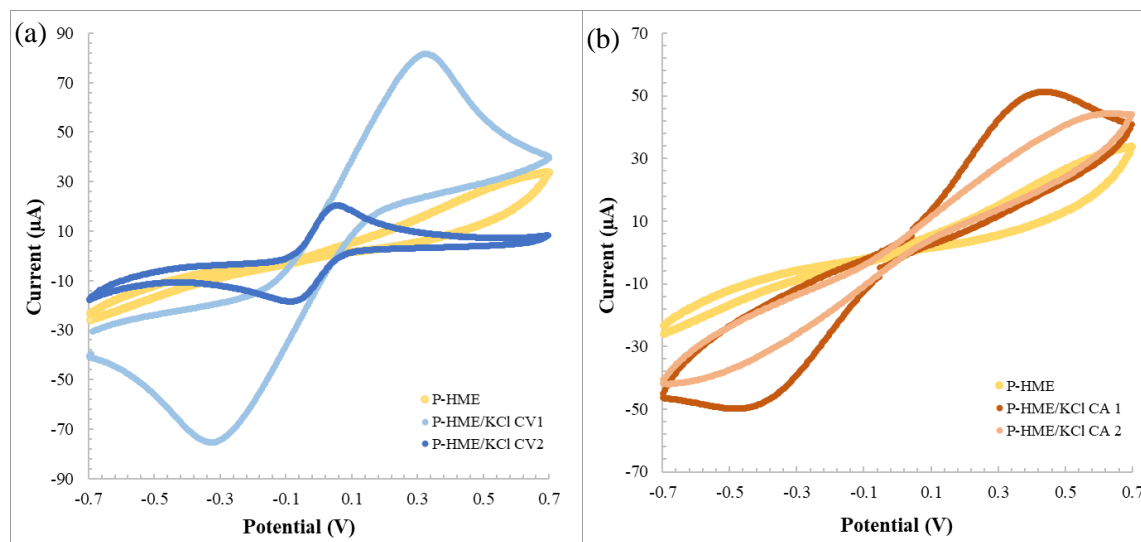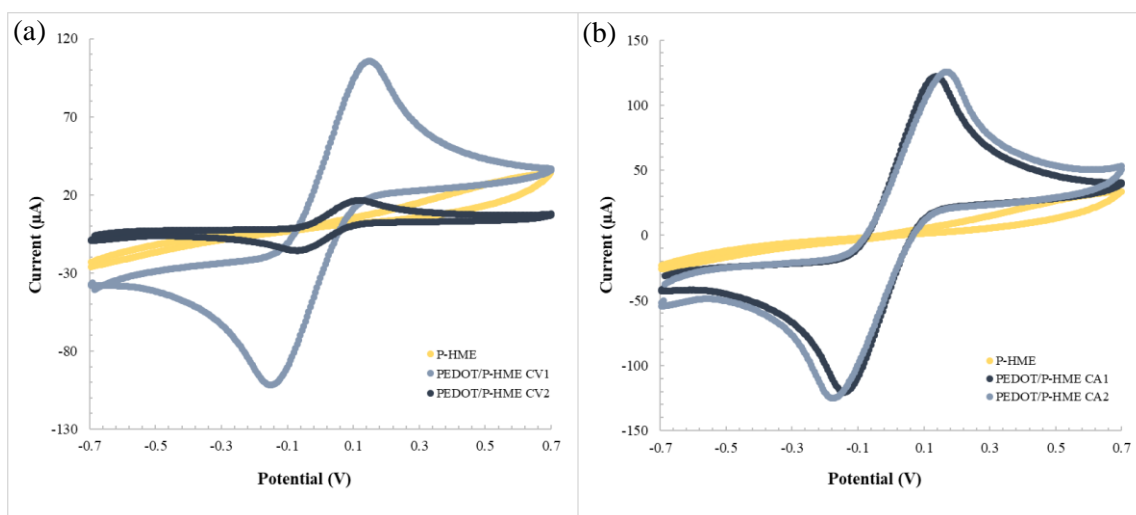

Figure 3.12 - Pre-treatment of P-HME with EDOT, (a) comparison between P-HME and two pre-treatments with CV; (b) comparison between P-HME and two pre-treatments with CA. Assessed in 5.0 mM $[Fe(CN)_6]^{3-}$ and 5.0 mM $[Fe(CN)_6]^{4-}$, in PBS buffer, pH 7.2

The CV fixed parameters were the number of cycles (3) and the scan rate (100 mV/s). CV1 as a range [-0.3; +1] V and CV2 [-0.3; +1.2] V. As can be seen, a bigger range, forms smaller and closer peaks.

To reduce the time spent on the CV, a CA pre-treatment was made setting voltage at 1 V and changing the time. With 10 s (CA 1), the peaks showed a better behaviour, but the increase of time to 30 s (CA2) led to a bigger layer of poly(EDOT) and the peaks were disposed to get further apart.

As can be seen in Annex H (Figure H.0.7), even with the chosen PEDOT treatment, the results after consecutive readings were not similar. This had to be justified by a constant change of material on the WE, that may have been generated by the lixiviation of material from the WE to the solution or by the entrance of external species, that could diffuse back (e.g. the reaction of EDOT monomers remaining within the polymeric layer).

Due to the existence of other type of electrodes that showed better results and considering this type was not electrochemically stable, no further studies were made.

3.3.2) Carbon Ink

3.3.2.1) Pre-treatment

Analogous to previous studies, these also started by readings in blank conditions to ensure similarity between several samples. These readings showed that even the CI-HME presented variances, which can be seen in Figure 3.13 by comparison of CV and EIS data.
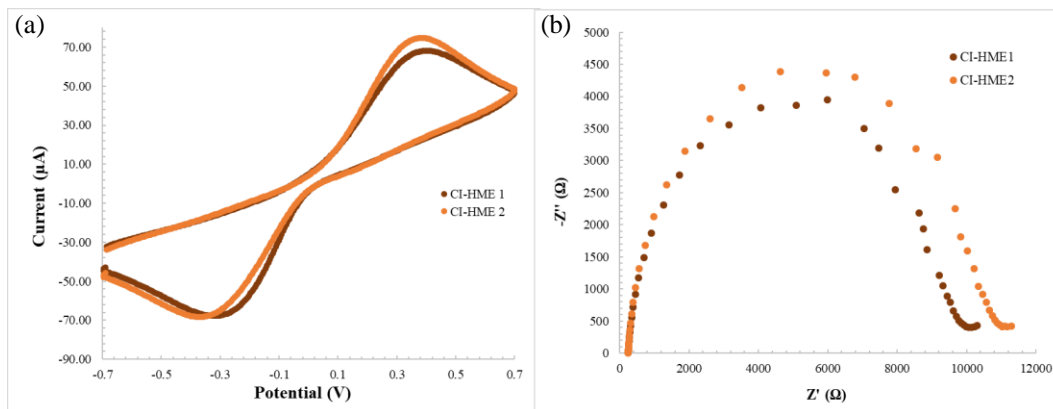
Figure 3.13- Comparison of two chips (a) CV reading of CI-HME1 and CI-HME2, (b) EIS reading of CI-HME1 and CI-HME2. Assessed in 5.0 mM $[Fe(CN)_6]^{3-}$ and 5.0 mM $[Fe(CN)_6]^{4-}$, in PBS buffer, pH 7.2.

Nonetheless, similar CI-HMEs were chosen and a procedure that could work for all of these was implemented. By analysing the CV graph, the oxidation and reduction peaks are seen widely separated, with peaks centred at approximately -0.3 V and +0.4 V for the HME-1 and -0.35 V and +0.37 V for the HME-2. Thus, we have a *quasi-reversible* behaviour in both HMEs, considering the current ratio is different from one and the voltage separation is higher than 59 mV.

The Nyquist plot in EIS showed a semicircle portion at high frequencies and a narrow linear portion at low frequencies. The semicircle at higher frequencies corresponds to the electron-transfer-limited process, and the linear portion at lower frequencies represents the diffusion-limited process. Overall, the R_{CT} values so obtained are too high.

In order to get better conditions for an electrochemical sensor and considering that EDOT modification was selected as the pre-treating stage of the P-HME, these CI-HMEs were also pre-treated similarly. For this purpose, the electrodes were treated by CA, with an EDOT solution for 10s, at 1V, to create a layer of polymer on top of the WE. The results can be seen in Figure 3.14. CV shows oxidation and reduction peaks of -0.1 V and 0.1 V, which indicate a *quasi-reversible* behaviour. The voltage separation is approximately 102 mV, which also indicated a *quasi-reversible* behaviour. Yet, these electrical features are by far the best conditions obtained with the HMEs and are also similar to the electrical features displayed by commercial screen-printed electrodes.

Figure 3.14- Pre-treatment of CI-HME: CV (a), EIS (b). Assessed in 5.0 mM $[Fe(CN)_6]^{3-}$ and 5.0 mM $[Fe(CN)_6]^{4-}$, in PBS buffer, pH 7.2

The electrochemical readings in EIS showed very little impedance values and no R_{CT} could be extracted from it, evidencing the high conductivity features of the system. The results also pointed out that the applied pre-treatment enabled higher homogeneity at the surface, by allowing similar results between different batches and a better electrochemical sensor response.
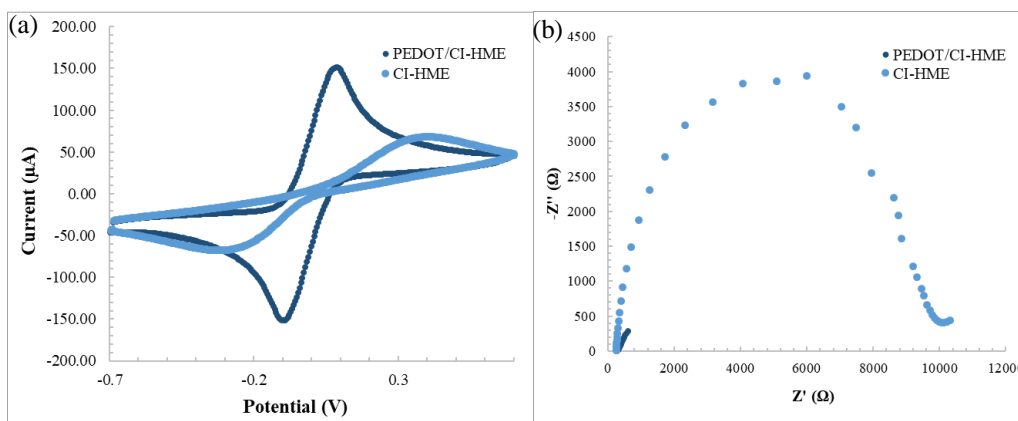
3.3.2.1)   MIP/NIP Fabrication

After pre-treatment, the HMEs were incubated in ATP for one hour. The ATP solution was an intermediate layer between PEDOT and the subsequent oPDA layer, working as a linker. The thiol group is expected to interact with EDOT, while the amine-aromatic ring is expected to establish a covalent bond to the MIP/NIP film, thereby ensuring that the imprinted polymeric layer is securely bond to the WE.

After the ATP incubation, the next step was the electropolymerization of oPDA, as shown in Figure 3.15. The technique selected for this process was CV, as there were several papers in literature using it, even with other monomers [30]. The formation of the oPDA film introduced additional barriers to the electron transfer properties of the redox probe. This resulted in an extra increase in the electron transfer resistance, reflected by further substantial increase in the charge transfer resistance (R_{CT}) compared to both HMEs in the previous state. The presence of Aβ-42 on the surface of the WE, after its adsorption, was confirmed by a R_{CT} increase, compared to the NIP HME-1 (Figure 3.15b). This increase was much more evident in the MIP, reflecting the presence of an insulating film plus the peptide.

For the removal process, the HMEs were incubated in a trypsin solution at 36 ºC for one hour. The main goal of this step was to remove the peptide from its imprinted site leaving the remaining polymeric network for the artificial antibody. Trypsin is highly active and stable with low cutting specificity and exhibits wide cleavage specificity.
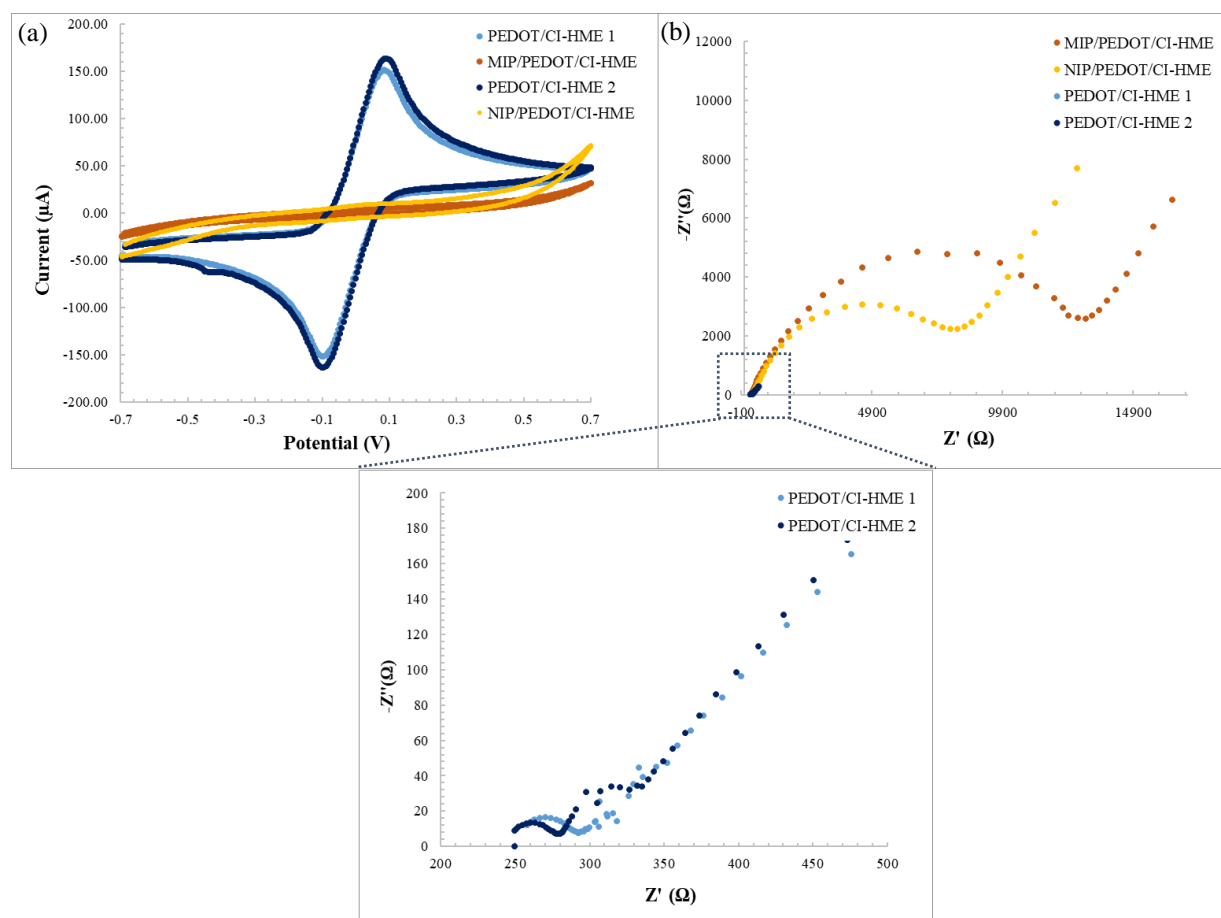
Figure 3.15 – Electrochemical readings of the sensing surfaces (MIP or NIP layers), by CV (a) and EIS (b) before the template removal. Zoomed section of the sensing surface before electropolymerization (PEDOT layer).

In some HMEs, a stable electrical response after consecutive readings could not be achieved. This could be due to the adsorption of trypsin into the matrix, so an extra step was added. Another incubation was made using oxalic acid for two hours, to ensure a proper protein removal.

With the protein removed, the resistance decreased substantially, suggesting that the peptide was successfully removed from the polymer. This decrease was abundantly perceptible in the MIP due to the existence of protein in it. In the NIP, these incubations did little to no difference, showing only a slight decrease in the R_{CT} after the incubations (Figure 3.16c). This decrease was probably related to the washout of small oligomer fragments from the surface or some adsorption in the matrix.

CV assays are consistent with the EIS results, as can be seen in Figure 3.16. The redox probe showed typical peak-to-peak potential separation values on both the chips with EDOT. The subsequent adsorption of the peptide promoted a peak decrease and a shift potential to higher values, confirming the presence of an additional element on the WE. After the polymerization, the peak currents dropped to lower levels, confirming the formation of an insulating layer on top of the HME surface. After template removal, the peak currents recovered, confirming the exit of the peptide from the electrode's surface. The NIP values showed a similar behaviour, except after polymerization, where the redox peaks of the probe remained evident.

Figure 3.16- Electrochemical follow-up of the several modification steps of the CI-HME to produce NIP (a and c) and MIP (b and d) films, by EIS (c and d, Nyquist plots) and CV (a and b, cyclic voltammograms). Results from a solution of 5.0 mM $[Fe(CN)_6]^{3-}$ and 5.0 mM $[Fe(CN)_6]^{4-}$, in PBS buffer, pH 7.2.

3.3.2.2)   Analytical Performance of the Biosensor

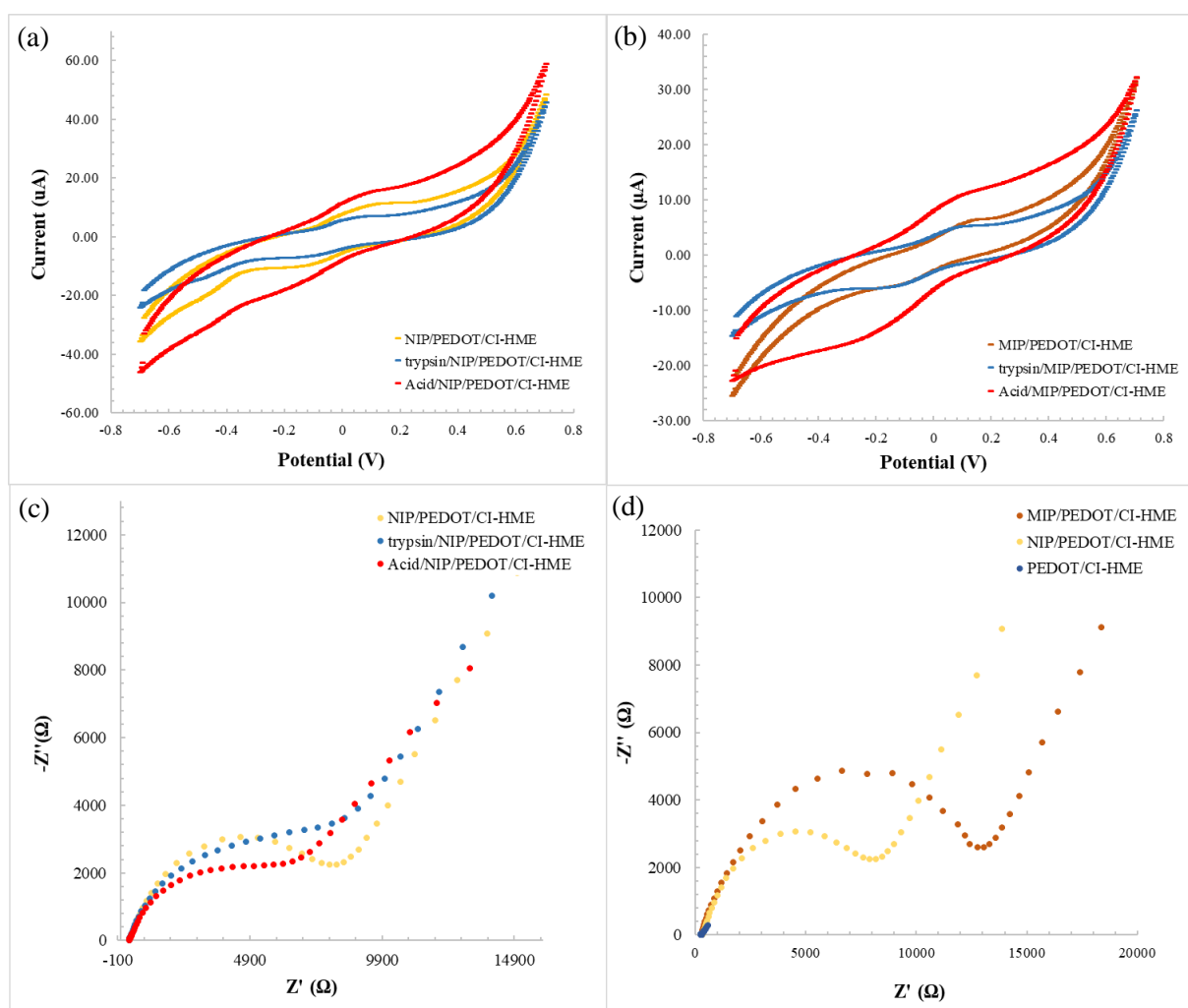In order to test the analytical performance of the biosensor under close-to-real conditions, it is important to establish a range for which the biomarker should be present, in a background medium that is close to a real analysis. In AD, there is still controversy on the amounts of Aβ-42 present in healthy and sick patients, thus this work considered that a healthy individual shows values close to 23.3 pg/mL [63]. In terms of background medium, the occurrence of Aβ-42 in cerebrospinal fluid and its relation to AD has been established so far, but its presence in serum emerges now as a possible less-invasive approach, thereby contributing to the early screening of the disease. Thus, the analytical response is first tested in PBS buffer (similar to serum) and in commercial serum (with a very complex composition, similar to real serum). Testing the HMEs in commercial serum shall also produce valuable data regarding the selectivity of the biosensor under conditions of real sample analysis. In addition, a calibration under "blank samples" led to a better tuning between samples and standard solutions, since the background composition in these solutions can be considered the same (or very similar).

PBS Buffer

The HME was calibrated by incubating standard solutions of Aβ-42 samples of increasing concentrations, prepared in PBS buffer. The obtained calibrations are shown in Figure 3.17a and Figure 3.17b, expressed in log concentration against the relative values to the signal in blank. The data were obtained after several 20 min incubations in PBS buffer.
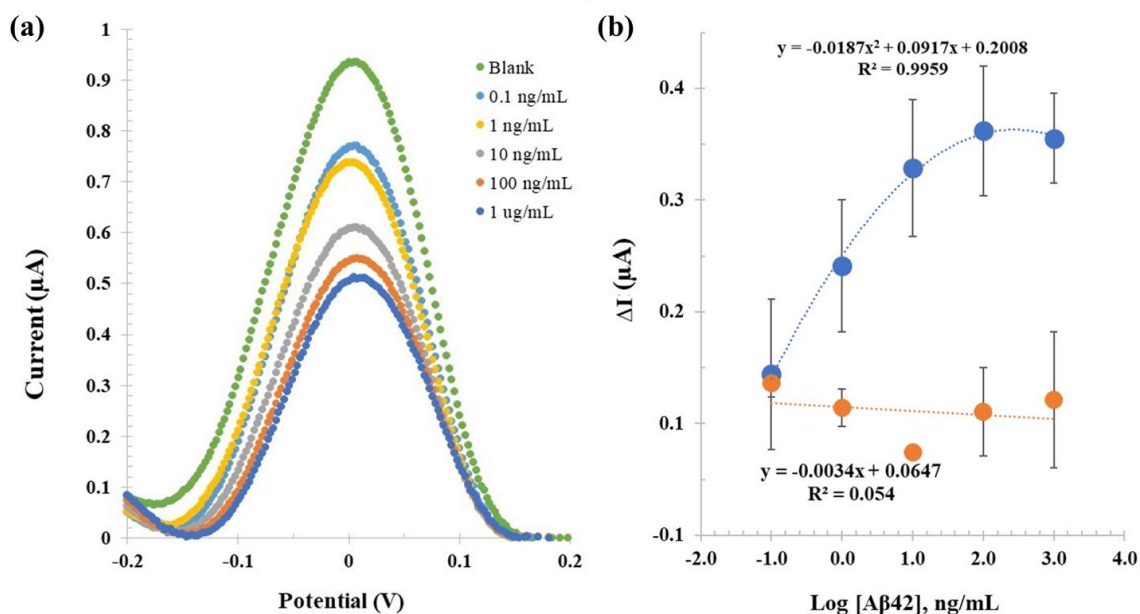
Figure 3.17- SWV (a) measurements of MIP/CI-HME based biosensor and the corresponding calibration curve (b), also compared to the NIP sensing layer. Different concentrations of Aβ42 (ng/mL) in PBS buffer. All assays were performed in 5.0 mM $[Fe(CN)_6]^{3-}$ and 5.0 mM $[Fe(CN)_6]^{4-}$, in PBS buffer, pH 7.2.

The SWV current responses were measured by varying the Aβ-42 concentration, as shown in Figure 3.17a. In MIP readings, the oxidation/reduction current responses were inversely proportional to the Aβ-42 concentration. The corresponding calibration was plotted with the current responses against the logarithm of Aβ-42 concentrations, shown in Figure 3.17b. In general, the peak current at 0 V decreased for higher concentrations of Aβ-42 diluted in PBS. The first incubation dropped the current values significantly, and the last three exhibited a little variation of the current, pointing out a tendency for saturation. Under optimized conditions, the MIP exhibited a dynamic response range between 0.1 ng/mL and 1 μg/mL. In contrast, the NIP showed a lower binding capacity in the same range of peptide concentration, as expected.

Overall, these results demonstrated that within the concentration range observed, the response of the MIP was dominated by the interaction of Aβ-42 with the rebinding sites, with negligible non-specific response observed.

Cormay Serum

To ensure the affinity with the peptide, calibration assays were conducted then in Cormay Serum. By performing the same process and using a complex matrix, similar behaviour to real samples can be ensured. The results obtained can be seen in Figure 3.18. The MIP was incubated first in serum and later in increasing concentrations of the peptide prepared in serum.
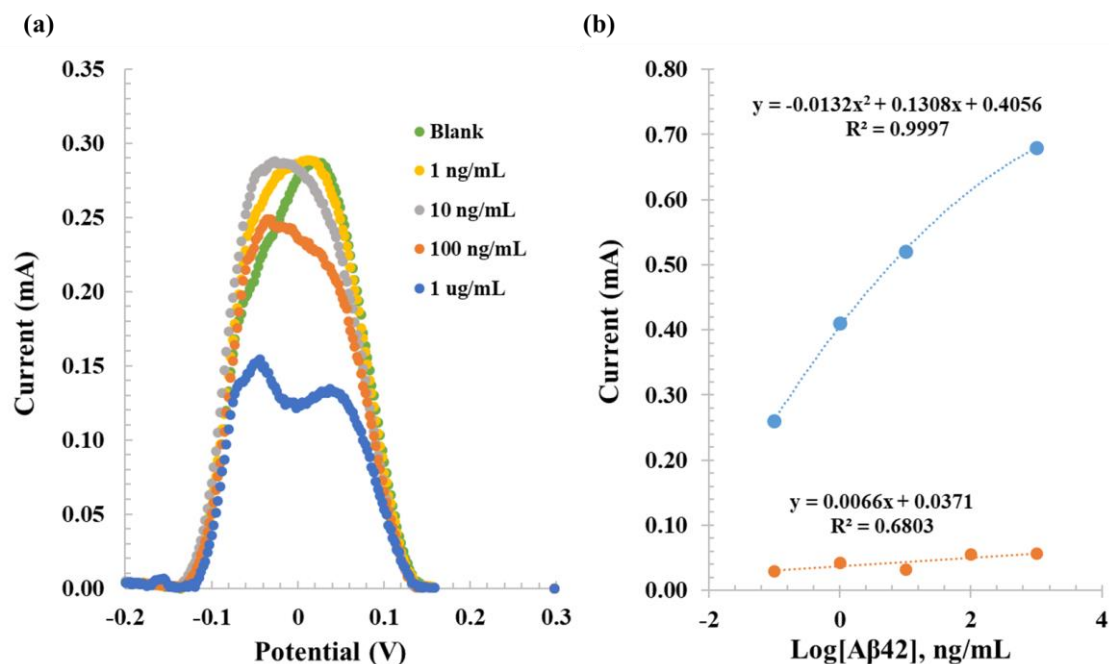
Figure 3.18 - SWV (a) measurements of MIP/CI-HME based biosensor in different concentrations of Aβ42 (ng/mL) in Cormay Serum, and the corresponding calibration curve (b, in blue), also comparing to the NIP (b, orange). All assays were performed in 5.0 mM $[Fe(CN)_6]^{3-}$ and 5.0 mM $[Fe(CN)_6]^{4-}$, in PBS buffer, pH 7.2.

Considering the blank incubations, an increase in peak current happened for the lowest concentration of Aβ-42 compared to the initial reading, which was not considered. Then the signal slowly decreased, showing little difference in the 0.1 ng/mL and 1 ng/mL concentrations, but dropping to significant values in the last two.

The NIP's response to serum is also shown in Figure 3.18b and can be compared to the response of the corresponding MIP, which is also consistent with the calibrations in PBS buffer. The NIP biosensor showed no response to the peptide after its blank was established, as it was expected.

Overall, a good agreement was found between added and found amounts of Aβ-42 and these results seemed promising for direct applications in POC context.

3.3.2.3)   Qualitative Analysis

The morphological and chemical characterization of the materials were made through SEM, Raman, and AFM analysis by direct analysis of the several materials. These results are displayed and discussed next.

<u>Raman Spectroscopy</u>

Raman spectra were recorded for CI-HME, PEDOT/CI-HME, MIP/Aβ-42/PEDOT/CI-HME (MIP film with Aβ-42), NIP/EDOT/CI-HME and MIP/-/PEDOT/CI-HME (after Aβ-42 removal). Results can be seen in Figure 3.19.

Figure 3.19- Raman Spectra of CI-HME, PEDOT/CI-HME, MIP/ Aβ-42/ PEDOT/CI-HME, NIP/PE-DOT/CI-HME and MIP/-/PEDOT/CI-HME

In general, all Raman spectra revealed the presence of a carbon-based matrix by showing two prominent visible peaks (G and D) at 1350 cm^{-1} and 1580 cm^{-1}, because all the materials relied on a carbon background. The G peak represented the bond-stretching vibrations o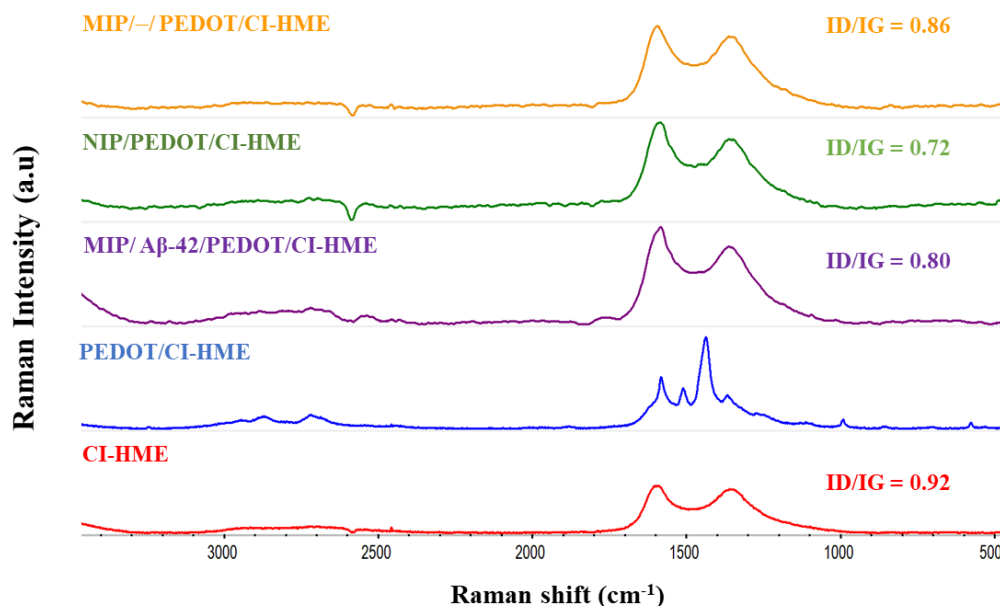f sp^2 hybridization carbon atoms, expressing the C=C stretching; the D peak expressed the vibrations of the carbon atoms of dangling bonds or sp^3 hybridized of carbon atoms, indicating the presence of disordered and/or defected in the carbon. The 2D peak represented the second order of the D band, involving a two-phonons lattice vibrational process, without the presence of any kind of disorder or defects [54].

In general, the intensity ratio (I_D/I_G) is characteristic of the extent of disorder present within the material: the higher the ratio, the lower the disorder [64]. The CI-HME was the starting material, with a ratio of 0.92. When EDOT was electropolymerized on top, two additional peaks appeared at this stage: one at 1442.5 cm^{-1}, the strongest one, and at 1506.2 cm^{-1} assigned to the C=C stretching. Overall, the changes occurring at the Raman spectra upon EDOT electropolymerization confirmed the presence of PEDOT on top of the carbon electrode [29], [65].

The addition of a polymeric imprinted layer on the PEDOT is expected to contribute to disorder the sp^2 carbon system, leading to a higher ratio as seen in MIP/Aβ-42/PEDOT/CI-HME. The increase of the I_D/I_G ratio from 0.8 to 0.86 was promoted by the removal of the peptide and indicates a higher presence of defects in the structure, which are consistent with the template sites present in the MIP structure. The NIP showed the lowest ratio due to the absence of imprinted sites and therefore lowest defects in the structure.

Overall, the Raman spectra confirmed the surface modifications and the presence of the imprinting sites of the sensor.

SEM images were collected for all CI-HME, PEDOT/CI-HME, MIP/PEDOT/CI-HME, removal/NIP/PEDOT/CI-HME, removal/MIP/PEDOT/CI-HME materials, as shown in Figure 3.20 and Figure 3.21.
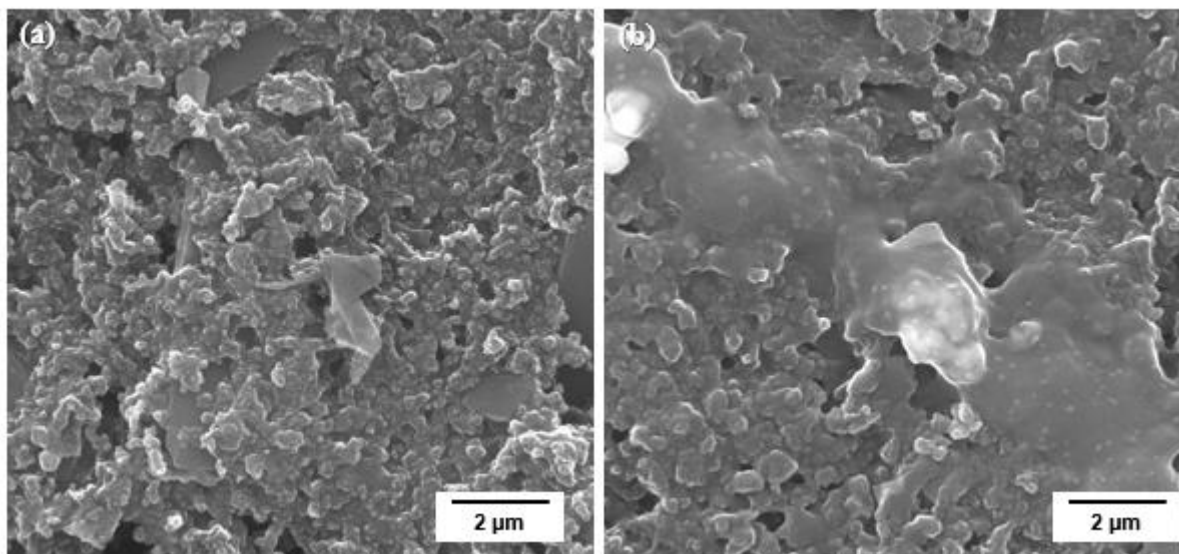
Figure 3.20 - SEM top view images (a) CI-HME (b) PEDOT/CI-HME
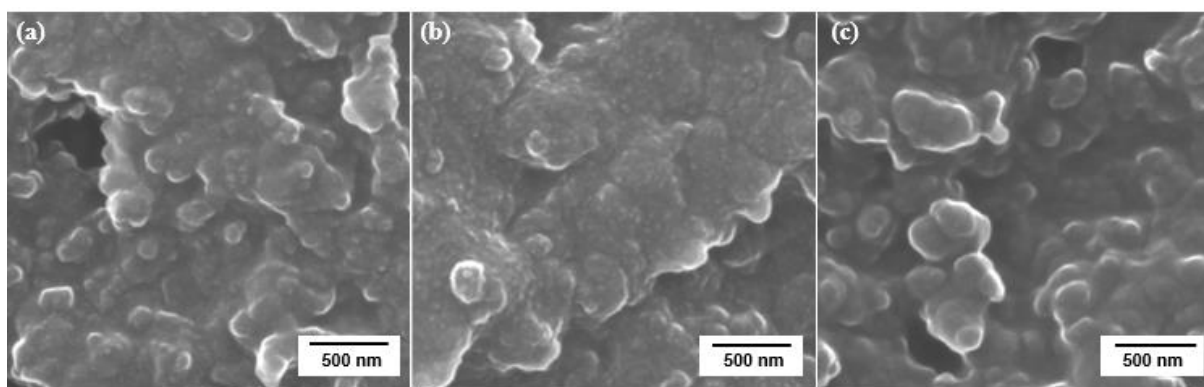
Figure 3.21 - SEM top view images (a) removal/NIP/PEDOT/CI-HME, (b) MIP/PEDOT/CI-HME and (c) removal/MIP/PEDOT/CI-HME

When doing the pre-treatment with EDOT, a noticeable film is created in the surface of the WE (Figure 3.20); this not only increased the conductivity, as created an even layer for the electrochemical steps further.

After electropolymerization the NIP (Figure 3.21a) and MIP (Figure 3.21b) images look quite similar, with the MIP showing less empty spaces, probably associated with the presence of the peptide. With the template removal process is possible to identify several empty spaces in the surface of the WE, as can be seen in Figure 3.21c.

AFM

Samples were also analyzed by AFM, morphologic changes can be seen in Figure 3.22 and Figure 3.23.
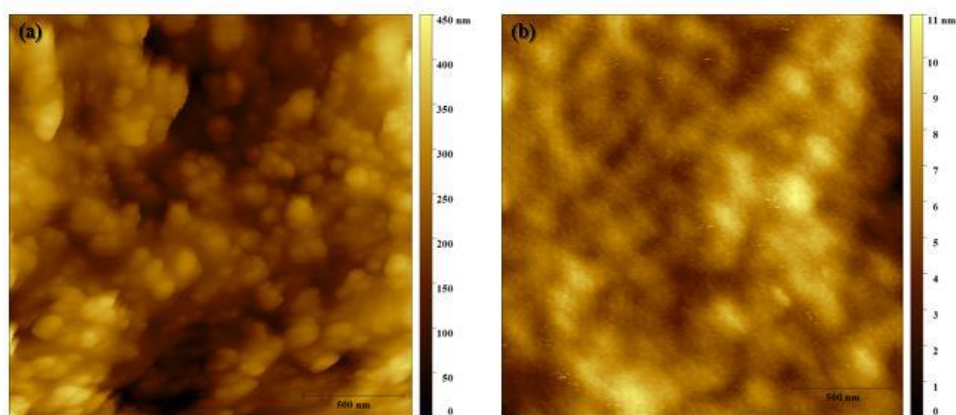
Figure 3.22 - AFM (a) CI-HME (b) CI-HME/PEDOT
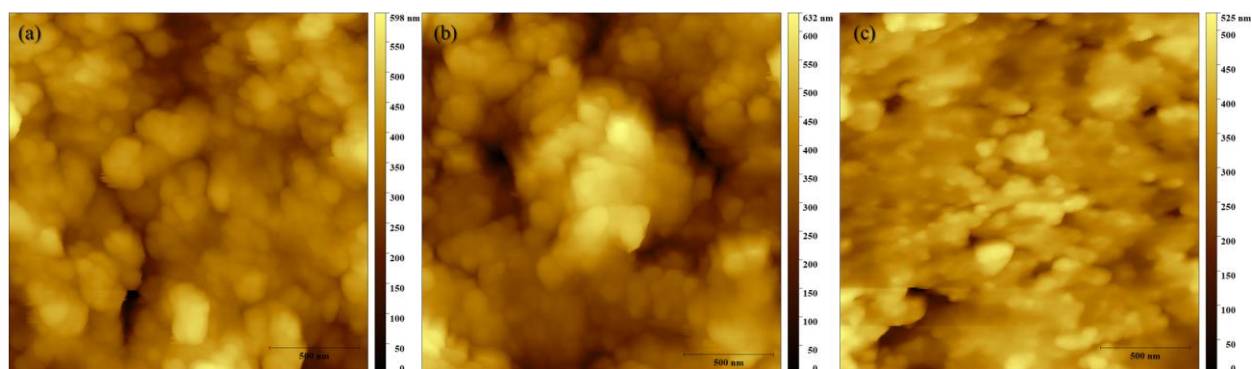
Figure 3.23 - AFM (a) MIP/PEDOT-CI-HME (b) removal/MIP/PEDOT-CI-HME, and (c) Aβ-42/MIP/PE-DOT-CI-HME

The morphological features resulting from each modification stage were studied on CI-HME surface, this surface revealed to be too rough as can be seen in Figure 3.22a. The ink was deposited by printing approaches and therefore its surface was too rough to allow the detection of any morphological changes promoted by a single monolayer modification, so an extra layer had to be added. With the PEDOT film its roughness was low enough to allow detecting changes related to the subsequent chemical modification.

The electropolymerization and subsequent formation of the MIP (Figure 3.23a) rendered significant changes in surface roughness (71.43 nm). The observed surface showed more roughness compared with the CI-HME/PEDOT (1.42 nm), which was consistent with the addition of a monolayer onto the WE surface.

After the treatment with trypsin and acid, surface roughness increased to 98.04 nm, thereby confirming the exit of the peptide and the presence of template sites (Figure 3.23b). With the addition of Aβ-42 these sites were no longer empty and surface roughness decreased to 58.48 nm (Figure 3.23c).

In general, the roughness of the MIP/PEDOT/CI-HME was about (71.43 nm), which was a higher value than the NIP material (68.29 nm), accounting the presence of the rebinding cavities.

Overall, the AFM data obtained along the different stages of electrode modification was consistent with the previous data, of electrochemical and chemical nature.

Finally, it was performed a cost analysis of the developed CI-HME. Table 3.2 shows the used materials, which present a cost of 0.02 € per sensor. It was not considered the cost related to the equipment used (laser machine and thermal plate).

Table 3.2 - Cost analysis of CI-HME

Material	Amount	Cost	Cost per unit
Office Paper	10 x 25 mm	1.9×10^{-3} €/m^2	4.75×10^{-7} €
Wax	2 x 10 x 25 mm	0,28 €/m^2	1.4×10^{-5} €
Lamination Pouch	10 x 25 mm	10.26 €/m^2	2.56×10^{-3} €
Carbon Ink	0.32 mg	65.2 €/kg	2.1×10^{-2} €

Total: 0.024 €

To have a better idea of the regular sensor cost, used for the same purpose as CI-HME, in Table 3.3 is presented a comparison between the most used sensors for electrochemical biosensing (Gold and Carbon screen-printed electrodes) and CI-HME.

Table 3.3 - Cost comparison between CI-HME and the two more common types of electrodes used for electrochemical biosensing (Gold and Carbon)

Electrodes	Cost per units
Carbon	1.87 €
Gold	2.87 €
CI-HME	0.02 €

4) Conclusion & Future Perspective

During this work, a paper-based electrochemical biosensor was developed with integration of a molecular imprinted polymer. Within the production of this biosensor, two types of material were used to create the electrodes: pencil and carbon ink. A study was conducted to determinate the effect of laser irradiation on both materials, and it revealed to have a strong impact on improving pencil's conductivity (from 619.98 $\Omega/\square$ to 29.91 $\Omega/\square$). Though this type of sensor did not work for electrochemical purposes, it opened a door for another applications, where laser treatment can be used to enhance inherent properties of materials. The project proceeded using carbon-based ink electrodes.

The main motivation of this work was the early diagnosis of Alzheimer's disease, as it is one of the main forms of dementia that affects millions of people worldwide. The studied analyte was a biomarker associated with AD, the peptide Aβ-42. The electrochemical sensor was incorporated with a MIP, since it is an alternative approach to natural antibodies. This MIP offers many advantages when compared to natural antibodies since it has high chemical stability, overall easy fabrication and low production costs.

CI-HMEs, were coated with a layer of EDOT to improve their stability in further electrochemical assays. For the electropolymerization, a mixture of oPDA (a monomer) and Aβ-42 was used and generated bulk polymerization. Herein, bulk polymerization was selected, because the presence of rebinding sites at the surface is always ensured, regardless the thickness of the polymeric layer. The best parameters for electropolymerization were a potential of [-0.45; +0.8] V for 10 cycles, at 100 mV/s.

The process of Aβ-42 removal from the biosensing film was optimized by using a solvent that could not induce a modification on the MIP's surface. Trypsin was used first for its proteolytic action, capable of cleaving the peptide bonds in Aβ-42 and leading to the formation of smaller peptide fragments, which are easily extracted in buffer. Next, oxalic acid were used to remove adsorbed peptide materials on the surface (fragments of Aβ-42 and also trypsin itself). After the template removal visible sites were seen in both SEM and AFM analysis, which proved an effective removal.

Overall, the sensor showed good operational characteristics, in a range of 0.1 ng/mL to 1 µg/mL. It showed reproducibility, good response time and selectivity. As for analytical performance, the biosensor showed adsorption of the peptide within the desired physiologic parameters, considering that a healthy individual shows values close to 23.3 pg/mL.

In general, the presented biosensor showed simplicity in design, short measurement time, was reusable, and displayed good selectivity. In addition, taking into account its production, it is eco-friendly and an overall cheap but reproducible sensor. This promising new approach opens the horizons for the rapid diagnosis of biomarkers associated with AD or other diseases in care settings.

Thus, considering a future perspective, it would be important to perform tests on real samples and to have an established Aβ-42 level on healthy and sick individuals. For this work, it would be important to re-evaluate the biosensors that are MIP-based and repeat the assays in Cormay serum.

References

[1] S. Prabhulkar, R. Piatyszek, J. R. Cirrito, Z. Z. Wu, and C. Z. Li, "Microbiosensor for Alzheimer's disease diagnostics: Detection of amyloid beta biomarkers," *J. Neurochem.*, vol. 122, no. 2, pp. 374–381, 2012.

[2] N. Fandos *et al.*, "Plasma amyloid β 42/40 ratios as biomarkers for amyloid β cerebral deposition in cognitively normal individuals," *Alzheimer's Dement. Diagnosis, Assess. Dis. Monit.*, vol. 8, pp. 179–187, 2017.

[3] M. Sjögren *et al.*, "Tau and Abeta42 in cerebrospinal fluid from healthy adults 21-93 years of age: establishment of reference values.," *Clin. Chem.*, vol. 47, pp. 1776–1781, 2001.

[4] J. V. Rushworth, A. Ahmed, H. H. Griffiths, N. M. Pollock, N. M. Hooper, and P. A. Millner, "A label-free electrical impedimetric biosensor for the specific detection of Alzheimer's amyloid-beta oligomers," *Biosens. Bioelectron.*, vol. 56, pp. 83–90, 2014.

[5] J. Schuster and S. A. Funke, "Methods for the Specific Detection and Quantitation of Amyloid-β Oligomers in Cerebrospinal Fluid," *J. Alzheimer's Dis.*, vol. 53, no. 1, pp. 53–67, 2016.

[6] H. Hampel and K. Blennow, "CSF tau and β-amyloid as biomarkers for mild cognitive impairment," *Dialogues Clin. Neurosci.*, vol. 6, no. 4, pp. 379–390, 2004.

[7] X. Sui, J. Liu, and X. Yang, "Cerebrospinal fluid biomarkers of Alzheimer's disease," *Neurosci. Bull.*, vol. 30, no. 2, pp. 233–242, 2014.

[8] Z. Zhao *et al.*, "Label-free detection of Alzheimer's disease through the ADP3 peptoid recognizing the serum amyloid-beta42 peptide," *Chem. Commun.*, vol. 51, no. 4, pp. 718–721, 2015.

[9] X. R. Cheng, B. Y. H. Hau, A. J. Veloso, S. Martic, H. B. Kraatz, and K. Kerman, "Surface plasmon resonance imaging of amyloid-?? aggregation kinetics in the presence of epigallocatechin gallate and metals," *Anal. Chem.*, vol. 85, no. 4, pp. 2049–2055, 2013.

[10] J. Oh *et al.*, "A carbon nanotube metal semiconductor field effect transistor-based biosensor for detection of amyloid-beta in human serum," *Biosens. Bioelectron.*, vol. 50, pp. 345–350, 2013.

[11] Y. Wang, J. Ping, Z. Ye, J. Wu, and Y. Ying, "Impedimetric immunosensor based on gold nanoparticles modified graphene paper for label-free detection of Escherichia coli O157: H7," *Biosens. Bioelectron.*, vol. 49, pp. 492–498, 2013.

[12] Y. K. Yoo *et al.*, "A highly sensitive plasma-based amyloid-β detection system through medium-changing and noise cancellation system for early diagnosis of the Alzheimer's disease," *Sci. Rep.*, vol. 7, no. 1, pp. 1–10, 2017.

[13] D. R. Thévenot, K. Toth, R. A. Durst, and G. S. Wilson, "Electrochemical biosensors: Recommended definitions and classification," *Biosens. Bioelectron.*, vol. 16, no. 1–2, pp. 121–131, 2001.

[14] H. Li, W. Wang, Q. Lv, G. Xi, H. Bai, and Q. Zhang, "Disposable paper-based electrochemical sensor based on stacked gold nanoparticles supported carbon nanotubes for the determination of bisphenol A," *Electrochem. commun.*, vol. 68, pp. 104–107, 2016.

[15] C. Wang, J. Wang, D. Liu, and Z. Wang, "Gold nanoparticle-based colorimetric sensor for studying the interactions of β-amyloid peptide with metallic ions," *Talanta*, vol. 80, no. 5, pp. 1626–1631, 2010.

[16] D. D. Liana *et al.*, "Sintered gold nanoparticles as an electrode material for paper-based electrochemical sensors," *RSC Adv.*, vol. 3, no. 23, pp. 8683–8691, 2013.

[17] I. Krishnaperumal and R. Lakshmanan, "An Approximate Analytical Method for the Evaluation of the Concentrations and Current for Hybrid Enzyme Biosensor," *ISRN Phys. Chem.*, vol. 2013,

pp. 1–12, 2013.

[18]   D. P. Addy and T. D. Gehman, "Bioelectronics: Biosensors," pp. 9–12, 2011.

[19]   D. Grieshaber, R. MacKenzie, J. Vörös, and E. Reimhult, "Electrochemical biosensors - Sensor principles and architectures," *Sensors*, vol. 8, no. 3, pp. 1400–1458, 2008.

[20]   E. Núnez-Bajo, M. C. Blanco-López, A. Costa-García, and M. T. Fernández-Abedul, "In situ gold-nanoparticle electrogeneration on gold films deposited on paper for non-enzymatic electrochemical determination of glucose," *Talanta*, vol. 178, pp. 160–165, 2018.

[21]   F. Tehrani and B. Bavarian, "Facile and scalable disposable sensor based on laser engraved graphene for electrochemical detection of glucose," *Sci. Rep.*, vol. 6, 2016.

[22]   A. R. Cardoso, F. T. C. Moreira, R. Fernandes, and M. G. F. Sales, "Novel and simple electrochemical biosensor monitoring attomolar levels of miRNA-155 in breast cancer," *Biosens. Bioelectron.*, vol. 80, pp. 621–630, 2016.

[23]   H. A. Abdulbari and E. A. M. Basheer, "Electrochemical Biosensors: Electrode Development, Materials, Design, and Fabrication," *ChemBioEng Rev.*, vol. 4, no. 2, pp. 92–105, 2017.

[24]   D. De Souza, S. A. S. Machado, and L. A. Avaca, "Voltametria de onda quadrada. Primeira parte: Aspectos teóricos," *Quim. Nova*, vol. 26, no. 1, pp. 81–89, 2003.

[25]   D. A. C. Brownson and C. E. Banks, *The Handbook of Graphene Electrochemistry*. 2014.

[26]   A. Bossi, F. Bonini, A. P. F. Turner, and S. A. Piletsky, "Molecularly imprinted polymers for the recognition of proteins: The state of the art," *Biosens. Bioelectron.*, vol. 22, no. 6, pp. 1131–1137, 2007.

[27]   G. V. Martins, A. C. Marques, E. Fortunato, and M. G. F. Sales, "8-hydroxy-2′-deoxyguanosine (8-OHdG) biomarker detection down to picoMolar level on a plastic antibody film," *Biosens. Bioelectron.*, vol. 86, pp. 225–234, 2016.

[28]   F. T. C. Moreira, S. Sharma, R. A. F. Dutra, J. P. C. Noronha, A. E. G. Cass, and M. G. F. Sales, "Protein-responsive polymers for point-of-care detection of cardiac biomarker," *Sensors Actuators, B Chem.*, vol. 196, pp. 123–132, 2014.

[29]   A. P. M. Tavares and M. G. F. Sales, "Novel electro-polymerized protein-imprinted materials using Eriochrome black T: Application to BSA sensing," *Electrochim. Acta*, vol. 262, pp. 214–225, 2018.

[30]   R. S. Gomes, F. T. C. Moreira, R. Fernandes, and M. F. Goreti Sales, "Sensing CA 15-3 in point-of-care by electropolymerizing O-phenylenediamine (oPDA) on Au-screen printed electrodes," *PLoS One*, vol. 13, no. 5, pp. 1–19, 2018.

[31]   M. Irimia-Vladu, "'Green' electronics: Biodegradable and biocompatible materials and devices for sustainable future," *Chem. Soc. Rev.*, vol. 43, no. 2, pp. 588–610, 2014.

[32]   S. Khan, L. Lorenzelli, and R. S. Dahiya, "Technologies for printing sensors and electronics over large flexible substrates: A review," *IEEE Sens. J.*, vol. 15, no. 6, pp. 3164–3185, 2015.

[33]   S. Kaneko *et al.*, "Choice of Paper for Multigraphene Growth on Lead Pencil Drawing," *Jpn. J. Appl. Phys.*, pp. 1–8, 2016.

[34]   D. Tobjörk and R. Österbacka, "Paper electronics," *Adv. Mater.*, vol. 23, no. 17, pp. 1935–1961, 2011.

[35]   J. H. Jin, J. H. Kim, S. K. Lee, S. J. Choi, C. W. Park, and N. K. Min, "A fully integrated paper-microfluidic electrochemical device for simultaneous analysis of physiologic blood ions," *Sensors (Switzerland)*, vol. 18, no. 1, 2018.

[36]   H. Shafiee *et al.*, "Paper and flexible substrates as materials for biosensing platforms to detect multiple biotargets," *Sci. Rep.*, vol. 5, no. i, pp. 1–9, 2015.

[37] R. Tortorich, H. Shamkhalichenar, and J.-W. Choi, "Inkjet-Printed and Paper-Based Electrochemical Sensors," *Appl. Sci.*, vol. 8, no. 2, pp. 288–304, 2018.

[38] C. Phillips, A. Al-Ahmadi, S. J. Potts, T. Claypole, and D. Deganello, "The effect of graphite and carbon black ratios on conductive ink performance," *J. Mater. Sci.*, 2017.

[39] Z. Q. Gong, A. N. A. Sujari, and S. Ab Ghani, "Electrochemical fabrication, characterization and application of carboxylic multi-walled carbon nanotube modified composite pencil graphite electrodes," *Electrochim. Acta*, vol. 65, pp. 257–265, 2012.

[40] H. T. Purushothama, Y. A. Nayaka, M. M. Vinay, P. Manjunatha, R. O. Yathisha, and K. V. Basavarajappa, "Pencil graphite electrode as electrochemical sensor for the voltammetric determination of Chlorpromazine," *J. Sci. Adv. Mater. Devices*, pp. 1–6, 2018.

[41] R.L. McCreery, "Advanced carbon electrode materials for molecular electrochemistry," *Chem. Rev.*, vol. 108, no. 7, pp. 2646–2687, 2008.

[42] A. N. Kawde, N. Baig, and M. Sajid, "Graphite pencil electrodes as electrochemical sensors for environmental analysis: A review of features, developments, and applications," *RSC Adv.*, vol. 6, no. 94, pp. 91325–91340, 2016.

[43] K. Chaisiwamongkhol, C. Batchelor-McAuley, S. V. Sokolov, J. Holter, N. P. Young, and R. G. Compton, "Optimising carbon electrode materials for adsorptive stripping voltammetry," *Appl. Mater. Today*, vol. 7, pp. 60–66, 2017.

[44] S. Kaneko *et al.*, "Multi Graphene Growth on Lead Pencil Drawn Sliver-Halide Print Paper Irradiated by Scanning Femtosecond Laser," *Jpn. J. Appl. Phys.*, pp. 1–9, 2015.

[45] Y. Chyan, R. Ye, Y. Li, S. P. Singh, C. J. Arnusch, and J. M. Tour, "Laser-Induced Graphene by Multiple Lasing: Toward Electronics on Cloth, Paper, and Food," *ACS Nano*, vol. 12, no. 3, pp. 2176–2183, 2018.

[46] W. Zhou *et al.*, "Laser-Direct Writing of Silver Metal Electrodes on Transparent Flexible Substrates with High-Bonding Strength," *ACS Appl. Mater. Interfaces*, vol. 8, no. 37, pp. 24887–24892, 2016.

[47] C. Fenzl, P. Nayak, T. Hirsch, S. Otto, H. N. Alshareef, and A. J. Baeumner, "Laser-scribed graphene electrodes for aptamer-based biosensing Laser-scribed graphene electrodes for aptamer-based biosensing," *ACS Appl. Mater. Interfaces*, pp. 1–9, 2017.

[48] A. Lamberti *et al.*, "New insights on laser-induced graphene electrodes for flexible supercapacitors: Tunable morphology and physical properties," *Nanotechnology*, vol. 28, no. 17, 2017.

[49] J. Lin *et al.*, "Laser-induced porous graphene films from commercial polymers," *Nat. Commun.*, vol. 5, pp. 1–8, 2015.

[50] M. Gobbi *et al.*, "Lipid-based nanoparticles with high binding affinity for amyloid-β1-42 peptide," *Biomaterials*, vol. 31, no. 25, pp. 6519–6529, 2010.

[51] Y. Kim, A. Sung, Y. Seo, S. Hwang, and H. Kim, "Measurement of hardness and friction properties of pencil leads for quantification of pencil hardness test," *Adv. Appl. Ceram.*, vol. 115, no. 8, pp. 443–448, 2016.

[52] R. N. Bhowmik, "Ferromagnetism in lead graphite-pencils and magnetic composite with $CoFe_2O_4$ particles," *Compos. Part B Eng.*, vol. 43, no. 2, pp. 503–509, 2012.

[53] A. E. Gamal *et al.*, "The effect of CO_2 and Nd:YAP lasers on CAD/CAM ceramics: SEM, EDS and thermal studies," *Laser Ther.*, vol. 25, no. 1, pp. 27–34, 2016.

[54] A. C. Ferrari, "Raman spectroscopy of graphene and graphite: Disorder, electron-phonon coupling, doping and nonadiabatic effects," *Solid State Commun.*, vol. 143, no. 1–2, pp. 47–57, 2007.

[55] F. Tuinstra and J. L. Koenig, "Raman Spectrum of Graphite," *J. Chem. Phys.*, vol. 53, no. 3, pp. 1126–1130, 1970.

[56] J. C. Lascovich, R. Giorgi, and S. Scaglione, "Evaluation of the sp2/sp3ratio in amorphous carbon structure by XPS and XAES," *Appl. Surf. Sci.*, vol. 47, no. 1, pp. 17–21, 1991.

[57] J. Díaz, G. Paolicelli, S. Ferrer, and F. Comin, "Separation of the sp3 and sp2 components in the C1s photoemission spectra of amorphous carbon films," *Phys. Rev. B*, vol. 54, no. 11, pp. 8064–8069, 1996.

[58] R. Navratil *et al.*, "Polymer lead pencil graphite as electrode material: Voltammetric, XPS and Raman study," *J. Electroanal. Chem.*, vol. 783, pp. 152–160, 2016.

[59] C. W. Foster *et al.*, *Pencil it in: Pencil drawn electrochemical sensing platforms*, vol. 141, no. 13. 2016.

[60] J. I. Gowda, G. S. Hurakadli, and S. T. Nandibewoor, "Pretreated Graphite Pencil Electrode Based Voltammetric Sensing of Albendazole," *Anal. Chem. Lett.*, vol. 7, no. 3, pp. 389–401, 2017.

[61] G. Parvizi-Fard, E. Alipour, P. Yardani Sefidi, and R. Emamali Sabzi, "Pretreated Pencil Graphite Electrode as a Versatile Platform for Easy Measurement of Diclofenac Sodium in a Number of Biological and Pharmaceutical Samples," *J. Chinese Chem. Soc.*, vol. 65, no. 4, pp. 472–484, 2018.

[62] Á. Torrinha, C. G. Amorim, M. C. B. S. M. Montenegro, and A. N. Araújo, "Biosensing based on pencil graphite electrodes," *Talanta*, vol. 190, pp. 235–247, 2018.

[63] M. C. Irizarry, "Biomarkers of Alzheimer Disease in Plasma," *NeuroRx*, vol. 1, no. 2, pp. 226–234, 2004.

[64] F. Withers, S. Russo, M. Dubois, and M. F. Craciun, "Tuning the electronic transport properties of graphene through functionalisation with fluorine," *Nanoscale*, vol. 6, p. 6, 2011.

[65] Z. Luo *et al.*, "Electronic structures and structural evolution of hydrogenated graphene probed by Raman spectroscopy," *J. Phys. Chem. C*, vol. 115, no. 5, pp. 1422–1427, 2011.

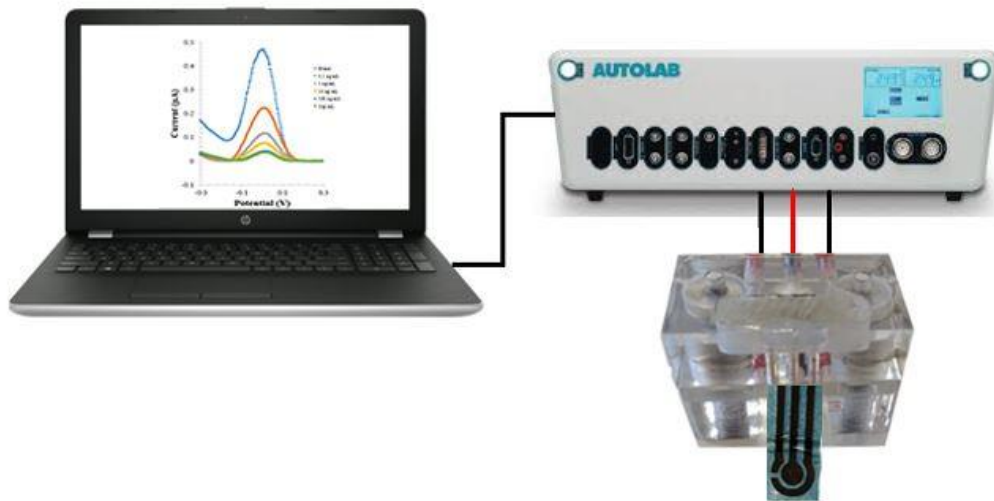# Supporting information

Annex A – Experimental Setup

Figure A.0.1- Experimental Setup

Annex B – Sheet Resistance according to type of pencil and amount of layers

Table B.0.1- Sheet Resistance according to type of pencil and amount of layers

Pencil	Layers	$\Omega/\square$	Pencil	Layers	$\Omega/\square$
9B	1	1592.998	**5B**	1	9983.996
	2	762.2824		2	3853.5596
	3	816.6664		3	4237.42
	4	619.9776		4	4754.068
8B	1	1642.3968	**4B**	1	11833.052
	2	541.574		2	6720.956
	3	593.692		3	4631.704
	4	488.0964		4	3108.952
7B	1	32730.104	**3B**	1	0
	2	16491.948		2	0
	3	3248.5376		3	0
	4	4303.5872		4	0
6B	1	3118.9224	**2B**	1	0
	2	2172.1876		2	0
	3	2074.2964		3	0
	4	1449.7868		4	0

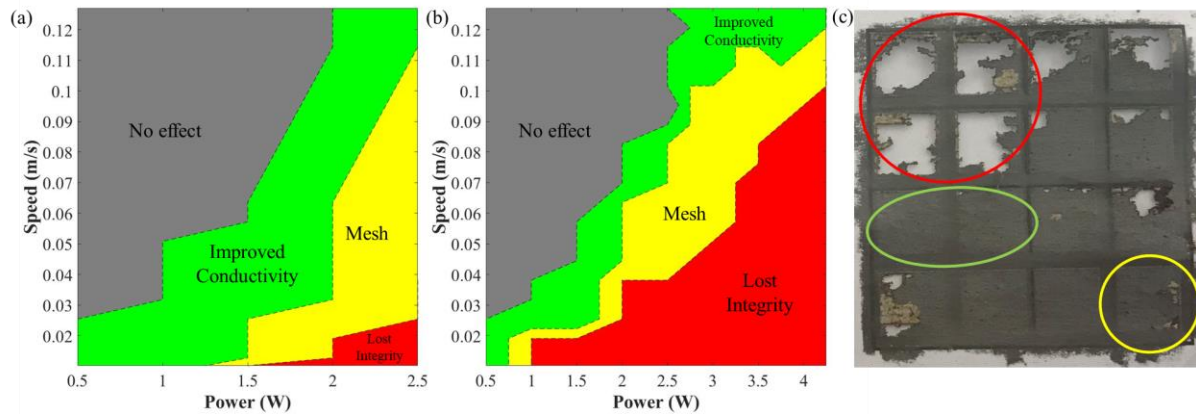## Annex C – Laser effect on pencil 9B with different paper substrates

Figure C.0.2 - Laser effect on pencil 9B with different paper substrates, (a) OP and (b) Whatman n°1. Plot of the 4 different Laser power and Speed regions that cause different after effect in the pencil/substrate. (c) Sample of OP with an example of lost integrity (market as red), mesh (marked as yellow) and improved conductivity (marked as green).

Annex D – CI-HME

Figure D.0.3 - Final CI-HME
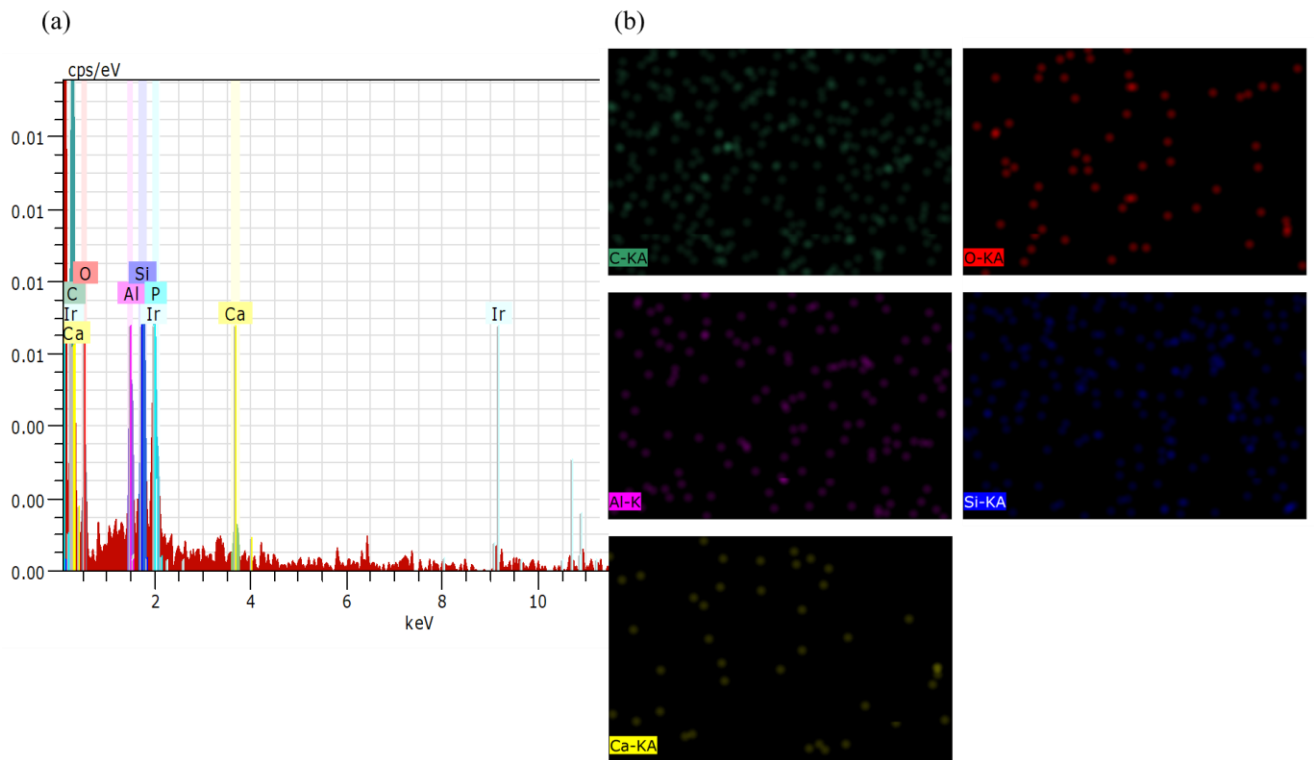
Annex E – EDS Mappings

(a)

(b)

Figure E.0.4- EDS analysis of a 9B pencil sample without laser treatment. (a) Cumulative spectrum of the EDS analysis, where the presence of iridium and phosphorous are due to the sample's coating. (b) EDS mappings of carbon, oxygen, aluminium, silicon and calcium.
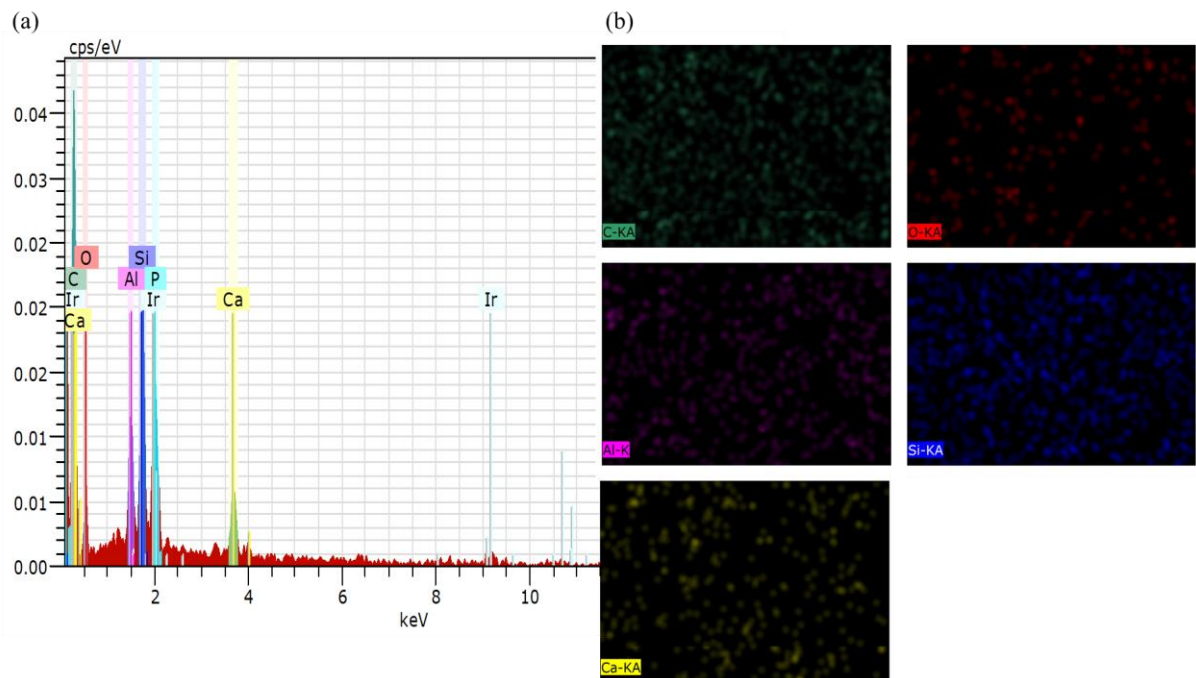
(a)

(b)

Figure E.0.5 - EDS analysis of a 9B pencil sample with laser treatment. (a) Cumulative spectrum of the EDS analysis, where the presence of iridium and phosphorous are due to the sample's coating. (b) EDS mappings of carbon, oxygen, aluminium, silicon and calcium.

Annex F – XPS

Table F.0.2 – XPS elemental composition (atomic %) of 9B pencil samples.

Sample: 9B pencil	Bond	% Concentration
Without laser treatment	C=C (sp^2)	76.61
	Pi-Pi*	5.28
	C-C (sp^3)	15.99
	C-OH, C-O-C	2.13
With laser treatment	C=C (sp^2)	90.16
	Pi-Pi*	6.21
	C-C (sp^3)	2.08
	C-OH, C-O-C	1.55

Annex G – NaCl Studies

In [61], a NaCl pre-treatment was performed in pencil-based chips, by CV using a range of [-2;+2]V for 10 cycles. Two scan-rate speeds were analysed 100 mV/s (CV1) and 50 mV/s (CV2) for this purpose. The wide potential range increased the time spent in this cleaning procedure and therefore CA was also tested. The best result with this technique was obtained using -0.5 V for 300 s, the results can be seen in Figure G.0.6.
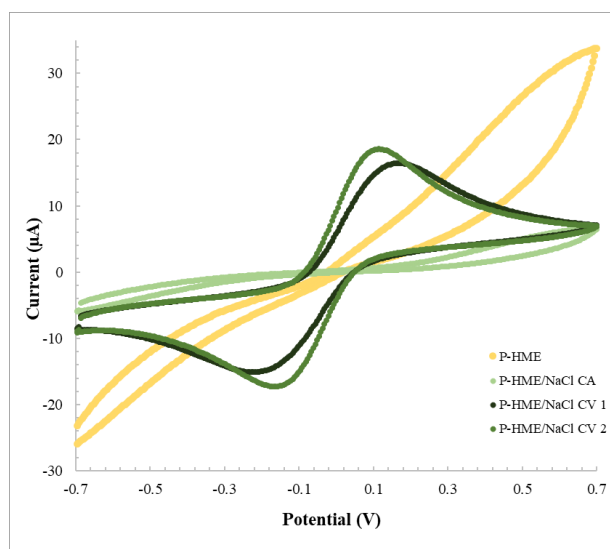

Figure G.0.6 - Pre-treatment of P-HME with NaCl, comparation between P-HME, a pre-treatment with CA and two pre-treatments with CV. Assessed in 5.0 mM $[Fe(CN)_6]^{3-}$ and 5.0 mM $[Fe(CN)_6]^{4-}$, in PBS buffer, pH 7.2

CV analysis showed better results for CV2 (slower scan rate), the oxidation and reduction peaks were of -0.17 V and +0.18 V, which indicated a *quasi-reversible* behaviour. The scan of the sample with CA pre-treatment displays worse electrical properties, therefore it is concluded that is a skippable step, at least for the NaCl solution.

For NaCl, the best conditions found were CV2, but as described in the KCl study, with EIS analysis the results continued to show inconstant readings with an increased R_{CT} tendency.
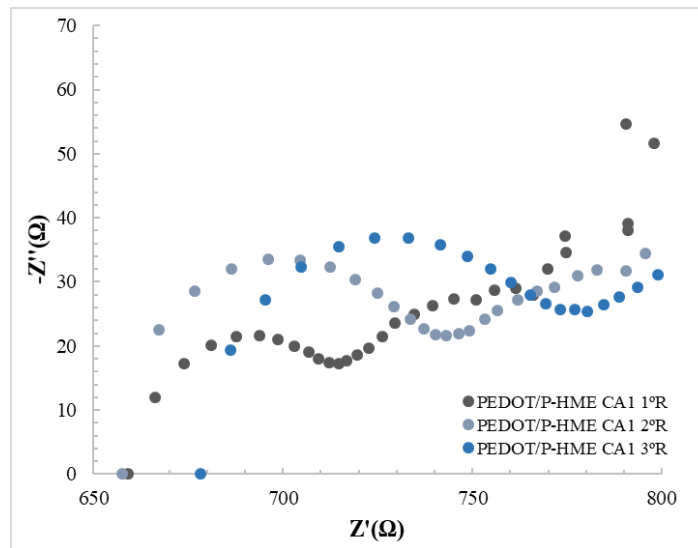
Annex H – EIS analysis of PEDOT layer on P-HME

Figure H.0.7 - EIS of PEDOT layer on P-HME, in consecutive readings.